https://doi.org/10.5194/egusphere-2026-5716
Preprint. Discussion started: 11 November 2026
© Author(s) 2026. CC BY 4.0 License.

The sparse matrix-based atmospheric moisture tracking (SMAT) model v1.0 for efficient diagnosis of global climatological moisture source–sink relationships

Yufeng Shan[1,2,3], Peng Qian[4], Kun Yang[5], Jiangfeng Wei[6], Dongdong Qiu[1,2,3], Fangyu Liu[7], Jun Ge[1,2,3]

[1]School of Atmospheric Sciences, Nanjing University, Nanjing, 210023, China
[2]Frontiers Science Center for Critical Earth Material Cycling, Nanjing University, Nanjing, China
[3]Joint International Research Laboratory of Atmospheric and Earth System Sciences, Nanjing University, Nanjing, China
[4]School of Atmospheric Physics, Nanjing University of Information Science and Technology, Nanjing, China
[5]Department of Earth System Science, Ministry of Education Key Laboratory for Earth System Modeling, Institute for Global Change Studies, Tsinghua University, Beijing, China
[6]School of Atmospheric Sciences, Nanjing University of Information Science and Technology, Nanjing, China
[7]LOCEAN-IPSL, IRD-CNRS-MNHN-Sorbonne Universités, Paris, France

Correspondence to: Jun Ge (junge@nju.edu.cn)

Abstract

Atmospheric moisture source–sink relationships characterize how moisture originating from evaporation in one region is transported through the atmosphere and ultimately contributes to precipitation in another. Quantifying these relationships is important for understanding moisture recycling, land–atmosphere interactions, and hydroclimatic teleconnections. However, existing moisture-tracking approaches remain computationally demanding for global and long-term climate applications. Here, we develop the sparse matrix-based atmospheric moisture tracking (SMAT) model that can efficiently diagnose global climatological moisture source–sink relationships. SMAT uses atmospheric moisture fluxes to describe moisture exchange among neighbouring grid cells under the local well-mixed assumption. These local transport relationships are assembled into a global sparse matrix, allowing atmospheric moisture redistribution to be solved directly without explicit step-by-step transport integration. This formulation substantially reduces the computational cost of global moisture source–sink diagnosis. Once the required transport fields have been constructed, the solution time depends primarily on spatial resolution rather than on the length of the analysis period. Global source–sink relationships can therefore be solved within hours or even minutes. We also evaluate SMAT against the multi-model-based global atmospheric moisture source–sink relationships (AMSSR) dataset and an additional Utrecht atmospheric moisture tracking (UTrack) dataset. Spatially, SMAT reproduces the major patterns of evaporation and precipitation recycling across grid, basin, and continental scales, together with the dominant land–ocean moisture source–sink pathways. Its deviations from AMSSR are generally comparable to, and in many cases smaller than, the corresponding UTrack–AMSSR deviations. Temporally, SMAT captures the climatological seasonal cycle of moisture recycling with performance comparable to that of UTrack. Overall, SMAT provides a computationally efficient framework for global atmospheric moisture source–sink diagnosis, particularly for high-resolution and large-ensemble climate applications.

https://doi.org/10.5194/egusphere-2026-5716
Preprint. Discussion started: 11 November 2026
© Author(s) 2026. CC BY 4.0 License.

1 Introduction

Atmospheric moisture source–sink relationships describe how atmospheric water is transported and redistributed through the hydrological cycle, linking moisture sources, primarily from evaporation, to sinks dominated by precipitation (van der Ent et al., 2010; Keys et al., 2012; van der Ent and Savenije, 2013; Zhang et al., 2025). Recent studies have indicated that anthropogenic drivers, particularly greenhouse-gas emissions and land-use change, are reshaping both local evaporation patterns and the large-scale transport of atmospheric moisture (Wang-Erlandsson et al., 2018; Findell et al., 2019; Gimeno et al., 2020; Staal et al., 2020b; Zan et al., 2024). These changes in turn reshape the spatial connectivity between moisture source and sink regions (Keys et al., 2012; Meier et al., 2021). Consequently, hydroclimatic changes originating in one region can propagate through atmospheric moisture transport and affect precipitation in remote downwind regions (Wang et al., 2018; Wei and Dirmeyer, 2019; Liu et al., 2023; Xie et al., 2024). Such effects have important implications for regional water availability (Cui et al., 2022), the occurrence and intensity of hydroclimatic extremes (Pranindita et al., 2022), and ecosystem stability (Rockström et al., 2023; Wang et al., 2025). For example, large-scale deforestation in the Amazon basin reduces evapotranspiration and weakens its function as a “biotic pump” (Makarieva and Gorshkov, 2007; Silvério et al., 2015), leading to decreased local precipitation while also affecting the stability of rainfall in remote downwind regions, such as the La Plata basin (van der Ent et al., 2010; Zemp et al., 2017; Cui et al., 2022), and potentially contributing to transitions from rainforest to savanna ecosystems (Lovejoy and Nobre, 2018; Staal et al., 2020a; Liu et al., 2025).

Atmospheric moisture tracking models have been widely used to quantify moisture source–sink relationships. These models simulate the transport and fate of atmospheric moisture based on the governing equations of atmospheric motion and moisture conservation. They can be broadly categorized into online and offline approaches. Online moisture-tracking approaches, such as the atmospheric water tracer (AWT) and water vapor tracer (WVT) schemes, are typically implemented within host atmospheric models, including global atmospheric general circulation models such as the Community Atmosphere Model version 5.1 (CAM5.1) and regional atmospheric models such as the Weather Research and Forecasting (WRF) model (Nusbaumer et al., 2017; Pan et al., 2017; Liu et al., 2023; Song et al., 2024), enabling moisture transport to be simulated consistently with atmospheric dynamics (Miguez-Macho et al., 2013; Insua-Costa and Miguez-Macho, 2018; Qian et al., 2024). Offline models, on the other hand, diagnose moisture transport using prescribed atmospheric fields from reanalysis or earth system model outputs (Dirmeyer and Brubaker, 1999; Sodemann et al., 2008; Qian et al., 2024). Representative approaches include Eulerian models such as WAM2layers (water accounting model-2layer) and Lagrangian particle dispersion models such as FLEXPART (FLEXible PARTicle dispersion model) and UTrack (Utrecht atmospheric moisture tracking model), which reconstruct moisture trajectories or fluxes from archived wind and humidity fields (Stohl and James, 2004; Tuinenburg and Staal, 2020; Kalverla et al., 2025).

https://doi.org/10.5194/egusphere-2026-5716
Preprint. Discussion started: 11 November 2026
© Author(s) 2026. CC BY 4.0 License.



However, existing moisture tracking approaches face substantial computational challenges for global, long-term, and large-ensemble climate applications. Online models, such as WRF-WVT, suffer from limited scalability, as each additional tagged source region introduces a new three-dimensional tracer field, leading to a prohibitive increase in memory usage and computational cost (Insua-Costa and Miguez-Macho, 2018; Insua-Costa et al., 2019; Dominguez et al., 2022). These computational bottlenecks constrain their application to regional scales or limited spatial domains. Offline approaches, while computationally more efficient than online methods, still require substantial computational resources to diagnose moisture transport and redistribution processes. In particular, Lagrangian models, such as FLEXPART, rely on large ensembles of air parcels, making them computationally intensive (Stohl and James, 2004; van der Ent et al., 2013; Vázquez et al., 2024). Eulerian approaches, while avoiding explicit trajectory calculations, also require extensive numerical calculations to resolve moisture fluxes at the global grid scale and thus remain computationally demanding when applied over extended temporal scales (Gimeno et al., 2012; van der Ent et al., 2013; Li et al., 2024). This computational burden limits their applicability for long-term and high-resolution analyses of global moisture source–sink relationships, and constrains their use in large ensemble experiments such as the Coupled Model Intercomparison Project Phase 6 (CMIP6), where computational efficiency is essential for diagnosing moisture source–sink relationships across multiple climate scenarios. Therefore, there is a clear need for an efficient and scalable method to diagnose global climate-scale moisture source–sink relationships.

In light of these challenges, we develop an efficient method, i.e., the sparse matrix-based atmospheric moisture tracking (SMAT) model, for diagnosing global climatic moisture source–sink relationships. From a Lagrangian perspective and based on the well-mixed assumption, SMAT reformulates the conventional moisture-tracking problem from step-by-step advection calculations of atmospheric moisture transport equations into the direct solution of a sparse matrix system. This formulation substantially reduces computational cost while retaining the physical basis of conventional moisture-tracking approaches, thereby enabling efficient diagnosis of global moisture source–sink relationships across climatic timescales. The remainder of this paper is structured as follows. Section 2 presents the methodology of SMAT, including the model principles and governing equations (Section 2.1), model inputs and outputs (Section 2.2), data preprocessing (Section 2.3), computational efficiency evaluation (Section 2.4), and self-validation and cross-dataset evaluation protocols (Section 2.5). Section 3 evaluates global moisture recycling and source–sink relationships, which are comprehensively detailed across grid (Section 3.1), basin (Section 3.2), and continental (Section 3.3) scales. Section 4 evaluates the ability of SMAT to capture the seasonal characteristics of moisture recycling at continental and basin scales, followed by concluding remarks in Section 5.

2 Method

SMAT is developed to efficiently diagnose climatic atmospheric moisture source–sink relationships while preserving the physical foundations of existing moisture-tracking approaches. Conventional moisture-tracking models generally adopt a hybrid framework in which moisture mixing is represented using local well-mixed assumptions, whereas moisture transport

https://doi.org/10.5194/egusphere-2026-5716
Preprint. Discussion started: 11 November 2026
© Author(s) 2026. CC BY 4.0 License.

between grid cells is resolved through explicit numerical integration of atmospheric moisture transport and water conservation equations (Dominguez et al., 2006; van der Ent et al., 2010; Kalverla et al., 2025). Although physically rigorous, these methods become computationally and memory-intensive for global, long-term, or high-resolution applications. To address this, SMAT retains the local well-mixed assumption but reformulates inter-grid moisture exchanges as a directional transfer network, enabling efficient diagnosis of global moisture source–sink relationships without explicit trajectory integration or numerical transport simulation. This reformulation markedly reduces the computational cost while retaining the physical consistency of established tracking approaches.

2.1 Fundamental principles and governing equations

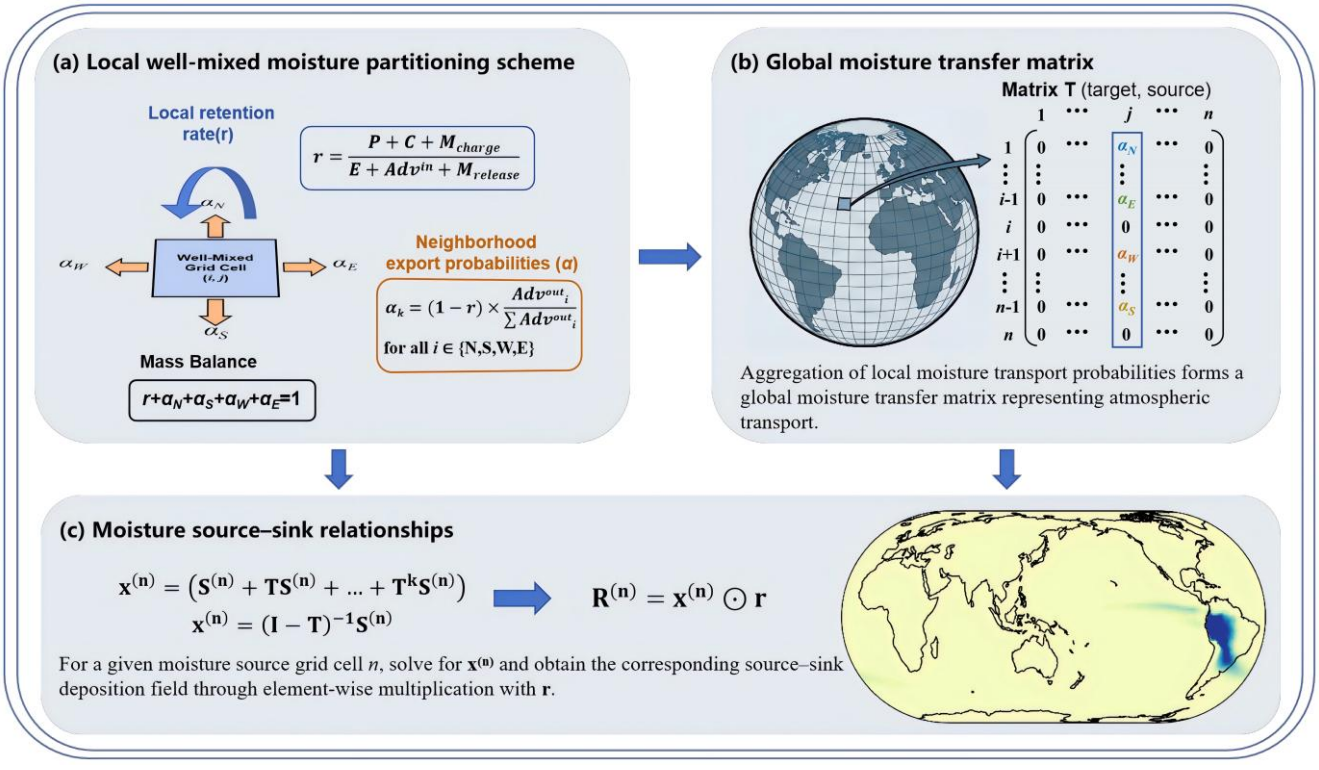


Figure 1. Schematic overview of SMAT. (a) Local well-mixed moisture partitioning within an individual grid cell, where incoming moisture is partitioned between local retention and lateral export pathways. (b) Construction of the global moisture transfer matrix **T** by linking local export probabilities among neighbouring grid cells. (c) Diagnosis of moisture source–sink relationships through the solution of the global transport system, yielding source-specific moisture distributions and the corresponding deposition fields.

https://doi.org/10.5194/egusphere-2026-5716
Preprint. Discussion started: 11 November 2026
© Author(s) 2026. CC BY 4.0 License.

2.1.1 Local well-mixed moisture partitioning scheme

SMAT begins with a local moisture partitioning scheme, as shown in Fig. 1. This scheme is based on the well-mixed assumption, under which water vapor from different sources is uniformly mixed within each grid-cell column, both horizontally and vertically. Consequently, all moisture components share identical probabilities of being partitioned into available sinks. Under the constraint of moisture conservation, these available sinks correspond to two categories of pathways for moisture within a given grid cell (i, j) at each time step: (1) horizontal export to any of the four neighbouring grid cells, and (2) local retention within the grid cell. This partitioning framework can be parameterized using a common set of partitioning probabilities, where a set of directional outward export probabilities α_k is associated with horizontal transport, and an internal retention probability r represents local sink processes. These partitioning probabilities satisfy the normalization constraint:

$$r + \alpha_N + \alpha_S + \alpha_W + \alpha_E = 1\,, \tag{1}$$

where $k \in \{\mathrm{N}, \mathrm{S}, \mathrm{W}, \mathrm{E}\}$ denotes the northward, southward, westward, and eastward directions, respectively.

The internal retention probability r measures the fraction of moisture entering a grid-cell atmospheric column that is retained locally. It is defined as the ratio of the local retention term S_{local} to the total moisture input to the column Q^{in}. The local retention term comprises three components: precipitation (P), condensation (C), and an increase in atmospheric moisture storage. Precipitation represents the removal of atmospheric moisture from the column through precipitation reaching the surface, whereas condensation represents its removal from the vapor phase through non-precipitating phase transitions. In addition to these processes, moisture may also be stored within the atmospheric column, with changes in precipitable water (PW) reflecting the associated storage tendency over the analysis period. A positive storage tendency, indicated by a sustained increase in precipitable water, represents net moisture accumulation within the column and is denoted as M_{charge}. Because this moisture remains in the column rather than being exported, it is included in S_{local} as locally retained moisture. The total moisture input Q^{in}, in contrast, consists of horizontal moisture advection into the grid cell (Adv^{in}), surface evaporation (E) and a decrease in atmospheric moisture storage. Here, Adv^{in} represents the moisture transported into the atmospheric column from surrounding grid cells, whereas E represents the moisture supplied from the surface through evaporation. A negative storage tendency, reflected by a decrease in precipitable water, indicates moisture release from atmospheric storage and is denoted as $M_{release}$. Since this moisture becomes available for atmospheric transport or precipitation, it is included in Q^{in}. The corresponding expressions for M_{charge} and $M_{release}$ are given as follows:

$$M_{charge} = max\left(\frac{dPW}{dt}, 0\right), M_{release} = max\left(-\frac{dPW}{dt}, 0\right), \tag{2}$$

Therefore, the internal retention probability is given by:

$$r = \frac{S_{local}}{Q^{in}} = \frac{P+C+M_{charge}}{Adv^{in}+E+M_{release}}\,, \tag{3}$$

https://doi.org/10.5194/egusphere-2026-5716
Preprint. Discussion started: 11 November 2026
© Author(s) 2026. CC BY 4.0 License.

According to atmospheric moisture conservation, the locally retained moisture S_{local} cannot exceed the total moisture input Q^{in}, ensuring that the calculated retention probability remains within the physically meaningful range of 0–1. After the local internal retention probability r has been determined, the remaining fraction of atmospheric moisture within a grid cell, $1-r$, is redistributed through horizontal advective export. Unlike conventional moisture-tracking models that explicitly simulate atmospheric moisture transport through step-by-step numerical integration of the governing transport equations, SMAT reformulates the moisture-tracking problem into a sparse matrix-based transport framework, enabling direct representation of moisture redistribution among grid cells. Within this framework, the moisture fraction available for horizontal transport is distributed among neighbouring grid cells according to the directional proportions of outward moisture fluxes across the four grid-cell boundaries. Specifically, the directional export probability α_k is defined as the product of the fraction of moisture available for horizontal transport $(1-r)$ and the fraction of the net outward moisture flux through boundary k (Adv_k^{out}) relative to the total horizontal outward moisture flux from the grid cell. Accordingly, α_k can be expressed as follows:

$$\alpha_k = (1-r)\frac{Adv_k^{out}}{\sum_{k\in\{N,S,W,E\}} Adv_k^{out}}, \quad (4)$$

2.1.2 Global moisture source–sink relationships

Building upon the local moisture partitioning scheme described above, the probabilistic moisture exchanges between neighbouring grid cells can be assembled into a global moisture transfer matrix **T**, which describes atmospheric moisture transport across the entire globe (Fig. 1b). When the global surface is discretized into N grid cells, **T** is defined as an $N\times N$ moisture transfer matrix, where the column index denotes the source grid cell and the row index denotes the receiving grid cell. Specifically, a matrix element $T_{m,n}$ represents the probability that atmospheric moisture originating from source grid cell n is transported to receiving grid cell m through moisture exchange among neighbouring grid cells. Since moisture transport occurs only between neighbouring grid cells at each transport step, each column of **T** contains only four non-zero elements, representing the directional export probabilities (α_N, α_S, α_W, α_E) from a given source grid cell to its neighbouring grid cells. Consequently, the sum of all the elements in column n equals the fraction of moisture available for horizontal transport:

$$\sum_{m=1}^{N} T_{m,n} = \alpha_N + \alpha_S + \alpha_W + \alpha_E = 1 - r_n, \quad (5)$$

Notably, periodic boundary conditions are imposed in the zonal direction by connecting the westernmost and easternmost grid cells, allowing continuous moisture transport across the longitudinal boundary. At the North and South Pole boundaries, meridional moisture transport is treated using a polar remapping scheme, whereby moisture crossing a pole re-enters the domain at the same polar latitude and the opposite longitude. This treatment ensures continuity of moisture transport over the spherical Earth while maintaining a uniform neighbour-connectivity structure throughout the global transport network.

Based on the global moisture transfer matrix **T**, the long-term redistribution of atmospheric moisture can be described as successive applications of the one-step transport operator. For any given grid cell n, we define the initial moisture source distribution as a column vector $\mathbf{S}^{(n)} \in \mathbb{R}^{N_{\text{grid}}}$, where moisture is injected at grid cell n while all other entries are zero. Through

https://doi.org/10.5194/egusphere-2026-5716
Preprint. Discussion started: 11 November 2026
© Author(s) 2026. CC BY 4.0 License.

repeated multiplication by **T**, this moisture is progressively transported across neighbouring grid cells, gradually spreading throughout the atmospheric circulation system (Fig. 1c). Accordingly, the resulting global moisture distribution $\mathbf{x}^{(n)} \in \mathbb{R}^{N_{\text{grid}}}$, representing the cumulative contribution of all possible transport pathways originating from grid cell *n*, can be expressed as follows:

$$\mathbf{x}^{(n)} = \mathbf{S}^{(n)} + \mathbf{T}\mathbf{S}^{(n)} + \mathbf{T}^2\mathbf{S}^{(n)} + \mathbf{T}^3\mathbf{S}^{(n)} + \cdots = \sum_{k=0}^{\infty} \mathbf{T}^k \mathbf{S}^{(n)} , \quad (6)$$

On a global scale, local moisture retention processes act as dissipation mechanisms, ensuring that the column sums of the non-negative transfer matrix T remain strictly less than 1 (Eq. 5). This property constrains the spectral radius of **T** to be less than 1, thereby ensuring the convergence of the matrix formulation and the existence of a unique steady-state solution. Under this condition, the cumulative contribution of atmospheric moisture redistribution through all possible transport pathways converges to a stable climatological source–sink distribution, which can be expressed in an equivalent linear algebraic form:

$$\mathbf{x}^{(n)} = (\mathbf{I} - \mathbf{T})^{-1}\mathbf{S}^{(n)} , \quad (7)$$

where $\mathbf{I} \in \mathbb{R}^{N_{\text{grid}} \times N_{\text{grid}}}$ denotes the identity matrix, and $(\mathbf{I} - \mathbf{T})^{-1}$ represents the inverse transport operator of the global moisture redistribution.

Finally, for a source grid cell *n*, its global moisture source–sink relationship is diagnosed by performing an element-wise multiplication between the corresponding global moisture distribution vector $\mathbf{x}^{(n)}$ and the moisture retention probability vector **r**. Specifically, for a target grid cell *m*, the moisture sink contribution originating from source grid cell *n* is calculated as follows:

$$R_{m,n} = x_m^{(n)} r_m , \quad (8)$$

where $\mathbf{R} \in \mathbb{R}^{N_{\text{grid}} \times N_{\text{grid}}}$ is the source–sink deposition matrix, in which each element $R_{m,n}$ quantifies the amount of moisture originating from a source grid cell *n* that is ultimately retained at a target grid cell *m*. The term $x_m^{(n)}$ denotes the steady-state moisture contribution at a target grid cell *m* induced by the source at a grid cell *n*. r_m denotes the local moisture retention probability of a grid cell m.

To link the diagnosed total retention to precipitation, an additional partitioning is introduced to account for the fraction of retained moisture that is converted into precipitation. Specifically, we define ρ_m as the precipitation coefficient ($\rho = \frac{P}{P+C+M_{charge}}$), which represents the fraction of locally retained moisture that is released as precipitation at a grid cell *m*. Accordingly, the precipitation-mediated source–sink deposition can be expressed as follows:

$$P_{m,n} = x_m^{(n)} r_m \rho_m , \quad (9)$$

where $\mathbf{P} \in \mathbb{R}^{N_{\text{grid}} \times N_{\text{grid}}}$ denotes the precipitation source–sink matrix, and $P_{m,n}$ represents the amount of precipitation at a grid cell *m* that is attributable to moisture originating from source grid cell *n*.

https://doi.org/10.5194/egusphere-2026-5716
Preprint. Discussion started: 11 November 2026
© Author(s) 2026. CC BY 4.0 License.

Overall, SMAT reformulates the long-term atmospheric moisture transport problem as a steady-state linear algebra system. By avoiding explicit time-marching integration of the governing partial differential equations, the model enables a direct sparse linear solution for the equilibrium moisture distribution. This formulation preserves the full source–pathway–sink information of moisture redistribution while achieving substantial gains in computational efficiency. As a result, SMAT is particularly well-suited for large-scale ensemble analyses, including multi-model datasets such as CMIP6, which require efficient diagnosis of moisture transport processes across extensive climate model archives.

2.2 Inputs and outputs

SMAT requires two categories of input fields to represent moisture redistribution within the atmosphere and exchanges between the land surface and atmosphere. Specifically, atmospheric moisture transport is represented using specific humidity and horizontal wind components on pressure levels, which are used to derive horizontal moisture fluxes among grid cells. These pressure-level data should include sufficient vertical levels to capture moisture transport in the lower troposphere, typically extending upward to at least 100 hPa. Furthermore, atmospheric fields should be provided at a daily or finer resolution, as monthly or longer averaging can cause cancellation of opposing inflow and outflow components across grid boundaries, resulting in inaccurate quantification of moisture exchanges among grid cells. Surface moisture exchange is then quantified using latent heat and precipitation fluxes. These surface fluxes can be provided at monthly or finer temporal resolutions, as cancellation of opposing components during temporal averaging is limited in most regions due to the dominance of positive latent heat flux associated with evaporation, with condensation becoming relevant mainly in snow- and ice-covered regions (e.g., Greenland and Antarctica).

SMAT outputs a four-dimensional moisture source–sink matrix (**R**) that describes global moisture contributions between source and sink cells. The first two dimensions of **R** correspond to the latitude and longitude indices of source grid cells, and the latter two dimensions represent the latitude and longitude indices of sink grid cells. For example, an element $R_{p,q,b,d}$ represents the amount of moisture released from the source grid cell (p, q) that is transported and retained at the sink grid cell (b, d).

2.3 Model preprocessing

To drive the moisture tracking model, the input data are subjected to rigorous preprocessing and physical diagnostic procedures. These procedures aim to construct a two-dimensional atmospheric moisture budget for each grid cell in the model domain, explicitly accounting for moisture sources and sinks, boundary fluxes, and storage tendencies.

https://doi.org/10.5194/egusphere-2026-5716
Preprint. Discussion started: 11 November 2026
© Author(s) 2026. CC BY 4.0 License.

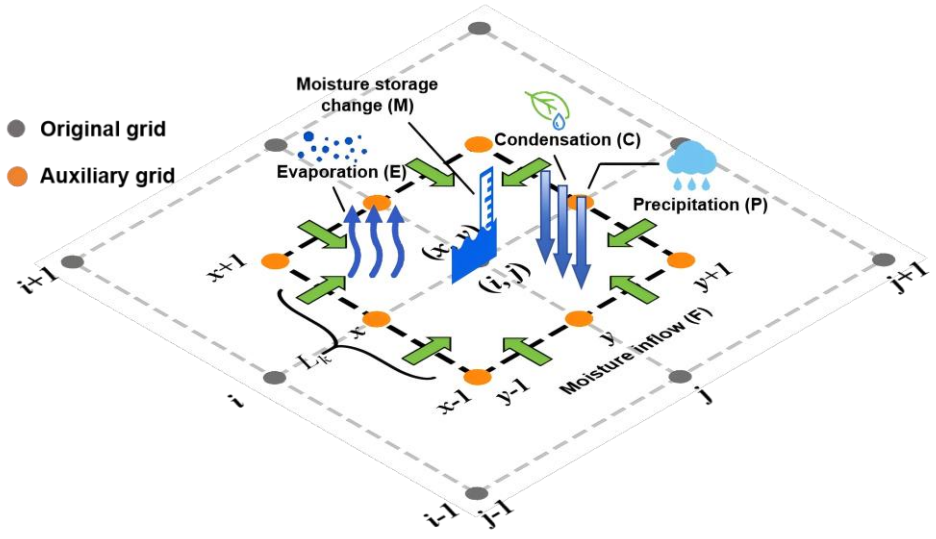


Figure 2. Conceptual illustration of the preprocessing procedures used to construct the atmospheric moisture budget for each grid cell in SMAT. Evaporation (*E*), condensation (*C*), precipitation (*P*), lateral moisture inflow through grid-cell boundaries, and changes in atmospheric water storage (*M*) are determined from the forcing data. To improve the estimation of inter-cell moisture transport, an auxiliary grid with twice the original horizontal resolution is introduced for boundary-flux calculations, and the resulting fluxes are subsequently mapped onto the original model grid.

2.3.1 Surface hydrological processes

Surface hydrological processes provide lower boundary conditions for the atmospheric moisture budget and include evaporation, condensation, and precipitation. These fluxes are derived from the forcing data and converted into area-integrated water fluxes for each model grid cell. Evaporation and condensation are determined from the sign of the surface latent heat flux (*LH*). A positive LH represents an upward latent heat flux from the land surface to the atmosphere and is associated with evaporation, whereas a negative LH represents a downward latent heat flux associated with condensation. For any grid cell (*i, j*) (Fig. 2), the corresponding area-integrated evaporation (*E*) and condensation (*C*) are calculated as follows:

$$E_{i,j} = A_{i,j}\, max\left(\frac{LH_{i,j}}{L_v}, 0\right),\ C_{i,j} = A_{i,j}\, max\left(-\frac{LH_{i,j}}{L_v}, 0\right), \quad (10)$$

where L_v is the latent heat of vaporization of water (2.45×10^6 J·kg^{-1}) and A is the geographical area of the grid cell. Precipitation is directly obtained from the forcing data. Consistent with the treatment of evaporation and condensation, the total precipitation (P) within a grid cell is calculated by multiplying the grid-cell precipitation flux (P') by the corresponding grid-cell area:

$$P_{(i,j)} = A_{(i,j)} P'_{(i,j)}\ , \quad (11)$$

https://doi.org/10.5194/egusphere-2026-5716
Preprint. Discussion started: 11 November 2026
© Author(s) 2026. CC BY 4.0 License.

2.3.2 Lateral boundary atmospheric moisture transport

Horizontal moisture transport across grid-cell interfaces governs the lateral redistribution of the tracked water mass and forms the basis of moisture transport in SMAT. Atmospheric variables from reanalysis and climate models are typically provided as cell-averaged values on a discrete grid. However, moisture exchange occurs across the interfaces between adjacent grid cells rather than at their centres. Consequently, directly using cell-averaged values to estimate interface fluxes introduces discretization errors, as the transport process is defined at cell boundaries while the state variables represent grid-cell averages. To reduce this inconsistency, an auxiliary grid with twice the original horizontal resolution is constructed to provide a more accurate representation of inter-cell moisture exchange and improve the estimation of boundary fluxes (Fig. 2).

Specific humidity (q) and horizontal wind components (u and v) are first interpolated from the original grid onto the auxiliary grid using bilinear interpolation, providing refined estimates of atmospheric variables along the boundaries of the original grid cells. For each auxiliary-grid point (x, y), the inflow moisture flux density (F) at pressure level p is evaluated according to the boundary of the original grid cell on which the point is located and the local wind direction:

$$F^{in}_{W_{x,y,p}} = max(u_{x,y,p}, 0)\ q_{x,y,p},\ F^{in}_{E_{x,y,p}} = max(-u_{x,y,p}, 0)\ q_{x,y,p},\ F^{in}_{S_{x,y,p}} = max(v_{x,y,p}, 0)\ q_{x,y,p},\ F^{in}_{N_{x,y,p}} = max(-v_{x,y,p}, 0)\ q_{x,y,p}\ , \quad (12)$$

After that, for each original grid cell (i, j), the total inflow through boundary k ($I_{k_{i,j}}$) at pressure level p is obtained by integrating the interpolated flux density along the corresponding grid-cell boundary:

$$I_{k_{i,j,p}} = \int_{L_{k_{i,j}}} F^{in}_k\, dl\ , \quad (13)$$

where $L_{k_{i,j}}$ denotes the length of the boundary of the grid cell (i, j), and $k \in \{\mathrm{N}, \mathrm{S}, \mathrm{W}, \mathrm{E}\}$. Boundary lengths are computed based on great-circle distances on the spherical Earth, with longitudinal grid spacing adjusted for latitude-dependent convergence toward the poles.

Along the vertical direction, the boundary fluxes are further integrated over all pressure levels above the land surface to obtain the total moisture inflow through each boundary ($Adv^{in}_{k_{i,j}}$):

$$Adv^{in}_{k_{i,j}} = \frac{1}{g}\int_{p_t}^{p_s} I_{k_{i,j}}(p)\, dp\ , \quad (14)$$

where g is the acceleration due to gravity, and p_s and p_t denote the surface and model-top pressures, respectively. The total moisture inflow into the grid cell (i, j) is then obtained by summing the contributions from the four boundaries:

$$Adv^{in}_{(i,j)} = Adv^{in}_{W_{i,j}} + Adv^{in}_{E_{i,j}} + Adv^{in}_{S_{i,j}} + Adv^{in}_{N_{i,j}}\ , \quad (15)$$

Since neighbouring grid cells share the same boundary, the moisture outflow through a given boundary ($Adv^{out}_{k_{i,j}}$) from the given grid cell (i, j) is equal to the moisture inflow through the corresponding boundary of the neighbouring grid cell.

https://doi.org/10.5194/egusphere-2026-5716
Preprint. Discussion started: 11 November 2026
© Author(s) 2026. CC BY 4.0 License.

2.3.3 Temporal aggregation and climatological averaging

SMAT is built upon the local well-mixed moisture assumption together with the assumption of a statistically stationary atmospheric transport pattern, whereby moisture within each grid cell is partitioned among outgoing pathways according to climatological transport probabilities. Although the final transport network represents a climatological mean state, these probabilities must be derived from atmospheric moisture fluxes diagnosed at sufficiently high temporal resolution. This is because the direction of moisture transport across a grid-cell boundary can vary over time. If low-temporal-resolution atmospheric fields, such as monthly mean winds, are used directly to calculate boundary fluxes, opposing inflow and outflow occurring within the averaging period may partially cancel each other, leading to an underestimation of the gross moisture exchange between neighbouring grid cells. Therefore, horizontal moisture fluxes are first diagnosed from the high-temporal-resolution atmospheric fields described in Section 2.3.2, with inflow and outflow components resolved separately at each time step. These moisture fluxes, together with the surface hydrological fluxes described in Section 2.3.1, are then integrated over each year and converted to a common unit of mm yr^{-1}. The resulting annual fluxes are subsequently averaged over all years in the analysis period to obtain the climatological mean moisture transport and surface hydrological flux fields used to construct the transfer network in SMAT.

2.4 Computational efficiency assessment

Since SMAT is formulated using climatological mean transport fields, it avoids the explicit time integration of transient moisture transport required by conventional moisture tracking models. Consequently, the computational cost of solving the global moisture transfer network depends primarily on the spatial resolution (i.e., the number of grid cells), but is largely independent of the temporal length of the analysis period and the temporal sampling frequency of the input datasets. Here, we evaluated the computational efficiency of SMAT across a range of spatial resolutions. All computational efficiency tests were performed on a single compute node equipped with one AMD EPYC 7551 32-core processor (64 threads), with all 64 threads used for the calculations. As shown in Fig. 3, the computational runtime of SMAT decreases rapidly with coarsening spatial resolution, spanning more than three orders of magnitude between 0.5°×0.5° and 2.5°×2.5°. At a spatial resolution of 0.5°×0.5°, solving the global moisture transfer network requires approximately 19 hours. Increasing the grid spacing to 1.0°×1.0° reduces the runtime to 36 minutes, corresponding to a speedup of more than 30-fold. Further coarsening decreases the runtime to 6 minutes at 1.5°×1.5°, 2 minutes at 2.0°×2.0°, and ultimately to only 50 seconds at 2.5°×2.5°. Overall, SMAT reduces the computational time for global climatological moisture source–sink diagnostics from weeks or even months to hours or even minutes, making high-resolution climatological diagnostics and large-ensemble applications computationally practical.

https://doi.org/10.5194/egusphere-2026-5716
Preprint. Discussion started: 11 November 2026
© Author(s) 2026. CC BY 4.0 License.

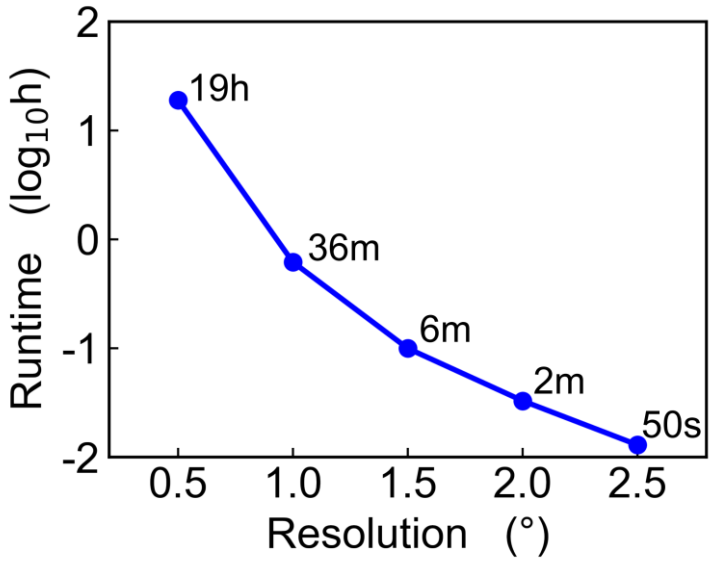


Figure 3. Computational runtime of SMAT as a function of spatial resolution. The blue line and markers show the runtimes required to solve the global moisture transfer network at spatial resolutions from 0.5°×0.5° to 2.5°×2.5°. The y-axis is shown on a base-10 logarithmic scale, while the labels above the markers indicate the corresponding absolute runtimes (h: hours; m: minutes; s: seconds).

2.5 Validation framework

In this study, the fifth-generation ECMWF reanalysis (ERA5) is used as the forcing dataset for SMAT, as it provides high-resolution atmospheric and surface reanalysis fields. Atmospheric forcing is obtained from daily pressure-level products, including specific humidity and horizontal wind components from 1000 to 1 hPa. Daily temporal resolution is selected to provide a balance between capturing meaningful moisture transport signals and reducing the storage demands associated with hourly data. Surface forcing is derived from hourly latent heat flux and precipitation fields to minimize the cancellation of intermittent positive and negative fluxes caused by temporal aggregation. Furthermore, the model is implemented at a 1° × 1° spatial resolution over the period 2008–2017 for subsequent cross-dataset evaluation.

2.5.1 Self-validation

Using the ERA5 reanalysis as forcing data, SMAT establishes climatological moisture source–sink relationships over the period 2008–2017. To evaluate model validity, we verified mass conservation by comparing the total moisture released from source grid cells with the total moisture received by sink grid cells, confirming that SMAT strictly conserves global moisture mass within numerical precision. Following this mass conservation assessment, we further assess the physical consistency of the precipitation sink distributions diagnosed using Eq. (9) by comparing them against the ERA5 precipitation data.

https://doi.org/10.5194/egusphere-2026-5716
Preprint. Discussion started: 11 November 2026
© Author(s) 2026. CC BY 4.0 License.

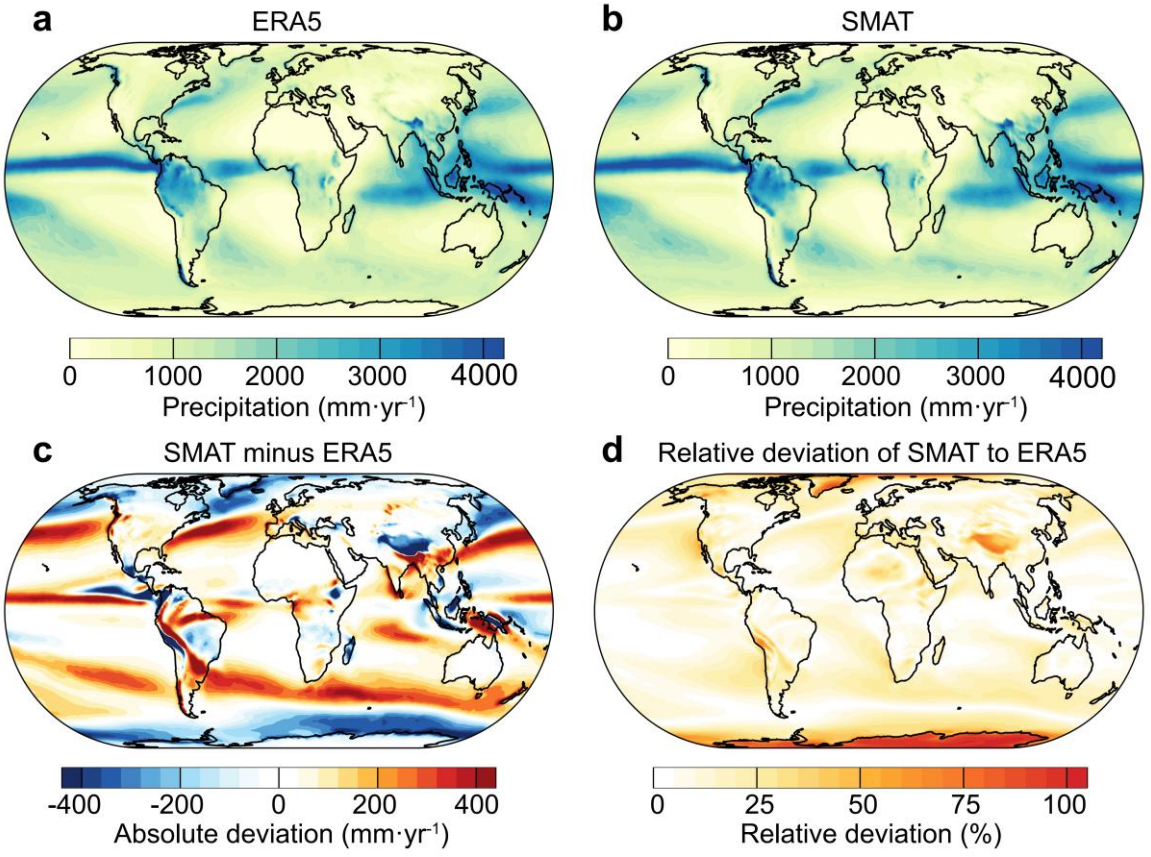


Figure 4. Global validation of annual mean (2008–2017) precipitation between SMAT and ERA5. Spatial distribution of annual mean precipitation (mm·yr⁻¹) derived from (a) the ERA5 reanalysis and (b) SMAT. (c) Absolute difference field calculated as SMAT minus ERA5. (d) Relative deviation (%) of SMAT relative to ERA5 baseline, defined as the absolute difference divided by the ERA5 climatological mean ($\frac{|SMAT-ERA5|}{ERA5} \times 100\%$).

As shown in Fig. 4a and b, SMAT generally reproduces large-scale patterns of global precipitation that are consistent with the ERA5 climatology. Major precipitation belts, including the tropical convergence zone (ITCZ), the Asian monsoon region, the Amazon Basin, and the Congo Basin, are well captured, while low-precipitation subtropical regions (e.g., Sahara, central and western Australia, and the eastern subtropical oceans) are also reasonably reproduced. Although SMAT successfully captures the large-scale precipitation distribution observed in ERA5, differences remain in the diagnosed precipitation magnitude. On the global scale, SMAT slightly overestimates the annual mean precipitation, yielding a global average of 1100 mm·yr⁻¹, compared with 1083 mm·yr⁻¹ from ERA5. Regionally, these precipitation biases exhibit distinct characteristics, with the largest discrepancies concentrated in the tropics and high latitudes of both hemispheres. In the tropics, alternating zonal bands of positive and negative biases suggest a slight meridional displacement of the ITCZ. In the Southern Hemisphere mid-to-high

https://doi.org/10.5194/egusphere-2026-5716
Preprint. Discussion started: 11 November 2026
© Author(s) 2026. CC BY 4.0 License.

latitudes, the zonally symmetric bias pattern, characterized by overestimation on the equatorward side and underestimation on the poleward side, indicates a modest equatorward shift of the Southern Ocean storm track. By contrast, biases in the Northern Hemisphere high latitudes are more heterogeneous, reflecting regional variations in storm track representation, particularly over the North Atlantic and North Pacific. Despite these regional differences, the relative deviations, calculated as $\frac{|SMAT-ERA5|}{ERA5} \times 100\%$, remain below 25% across most regions (Fig. 4d), indicating that biases in diagnosed precipitation are generally small relative to the background precipitation magnitude.

2.5.2 Cross-dataset evaluation framework

To further evaluate the performance of SMAT, we compare its results with benchmark moisture-tracking datasets and simulations from existing moisture-tracking models. We select the multi-model based global atmospheric moisture source–sink relationships (AMSSR) dataset as the primary reference, as it provides an optimal ensemble mean of three widely used moisture-tracking models (WAM2Layers, UTrack, and WaterSip). The AMSSR dataset is driven by the ECMWF Interim Reanalysis (ERA-Interim) and provides quarterly global moisture source–sink relationships from 1980 to 2018 at a spatial resolution of 1° × 1°. To further provide a reference for interpreting the magnitude of discrepancies between SMAT and AMSSR, an additional UTrack-based moisture source–sink dataset is considered to characterize inter-model differences among moisture-tracking approaches. UTrack, which serves as one of the three models for generating the AMSSR data, is driven by ERA5 and provides monthly climatological source–sink relationships averaged over 2008–2017 at the same spatial resolution. The deviation of UTrack from AMSSR therefore serves as a benchmark for the existing spread among moisture-tracking approaches. Specifically, for each grid cell, the absolute discrepancies between SMAT and AMSSR, $|\ D_{\mathrm{SMAT}}\ |=|\ X_{\mathrm{SMAT}} - X_{\mathrm{AMSSR}}\ |$, and between UTrack and AMSSR, $|\ D_{\mathrm{UTrack}}\ |=|\ X_{\mathrm{UTrack}} - X_{\mathrm{AMSSR}}\ |$, are directly compared, where X denotes the evaluated diagnostic variable (e.g., evaporation recycling ratio, precipitation recycling ratio, or moisture source–sink contribution). If $|D_{\mathrm{SMAT}}| < |D_{\mathrm{UTrack}}|$, the deviation introduced by SMAT is smaller than the disagreement between UTrack and the AMSSR ensemble, indicating that SMAT results remain within the range of discrepancies represented by existing moisture-tracking approaches. Otherwise, SMAT deviation exceeds this benchmark, implying that the discrepancies are larger than the current inter-model spread.

The cross-dataset evaluation focuses on the 2008–2017 climatology, corresponding to the overlapping period of the AMSSR and UTrack-based datasets. To facilitate a consistent comparison, SMAT was applied at a spatial resolution of 1° × 1° over the same period. While this aligns the temporal coverage and spatial resolution among the datasets, their atmospheric forcing remains different: AMSSR is driven by ERA-Interim, whereas both SMAT and UTrack are based on ERA5. Since the ERA-Interim atmospheric fields required to rerun SMAT and UTrack were not available in this study, a fully forcing-consistent comparison could not be achieved. To reduce the influence of forcing differences associated with surface moisture supply, SMAT- and UTrack-based source–sink relationships were therefore recalculated using the evaporation fields provided by

https://doi.org/10.5194/egusphere-2026-5716
Preprint. Discussion started: 11 November 2026
© Author(s) 2026. CC BY 4.0 License.

AMSSR. This places the three datasets on a common evaporation basis, while differences arising from the underlying atmospheric circulation fields remain. The following evaluation focuses on two aspects: the spatial characteristics of moisture recycling, including climatological patterns at the grid, basin, and continental scales and dominant land–ocean moisture source–sink relationships, and the temporal characteristics represented by the seasonal cycle of moisture recycling.

3 Global moisture recycling and source–sink relationships

3.1 Grid-scale moisture recycling

We first evaluate the ability of SMAT to characterize local moisture recycling using two key diagnostics: the evaporation recycling ratio and the precipitation recycling ratio (PRR). The evaporation recycling ratio (ERR) is defined as the fraction of moisture evaporated from a given grid cell that is eventually retained within the same grid cell after atmospheric transport:

$$ERR_n = \frac{R_{n,n}}{E_n}, \tag{16}$$

where $R_{n,n}$ represents the amount of moisture originating from evaporation in grid cell n and ultimately retained within the same grid cell, and E_n denotes the total evaporation from grid cell n. Conversely, the precipitation recycling ratio (PRR) is defined as the fraction of moisture retained within a given grid cell that originates from evaporation occurring within the same grid cell:

$$PRR_n = \frac{R_{n,n}}{\sum_{i=1}^{N} R_{n,i}}, \tag{17}$$

where $\sum_{i=1}^{N} R_{n,i}$ represents the total moisture retained within grid cell n from all source grid cells.

At the grid scale, both ERR and PRR exhibit pronounced spatial heterogeneity across the globe (Fig. 5a, b, c, d). SMAT reproduces the major recycling hotspots represented by the AMSSR reference dataset, including the Amazon and Congo basins, the Tibetan Plateau, the Southeast Asian monsoon region, and the Andes. This broad spatial agreement is also reflected in the global mean values. The area-weighted mean of the grid-cell ERR values is 1.93% in SMAT and 1.96% in AMSSR, while the corresponding mean PRR values are 1.88% and 1.76%, respectively. The largest departures from AMSSR occur primarily in hyper-arid regions. In particular, the extensive high ERR and PRR values over the Sahara Desert and North Africa in AMSSR are largely absent in SMAT, resulting in near-zero recycling ratios over these regions (Fig. 5e, f). Overall, SMAT underestimates ERR and PRR over approximately 37.2% and 38.3% of the global domain, respectively. Despite these regional discrepancies, SMAT–AMSSR differences are generally comparable to the inter-model differences represented by UTrack. The grid-cell area-weighted mean absolute deviations between SMAT and AMSSR are 0.95% for ERR and 0.78% for PRR, which are smaller than the corresponding UTrack–AMSSR values of 1.33% and 1.12%, respectively. Spatially, SMAT deviation from AMSSR is smaller than the corresponding UTrack deviation over 63.8% of the global domain for ERR and

https://doi.org/10.5194/egusphere-2026-5716
Preprint. Discussion started: 11 November 2026
© Author(s) 2026. CC BY 4.0 License.

60.8% for PRR. These results indicate that SMAT captures the dominant grid-scale patterns of local moisture recycling, with deviations remaining within the range represented by existing moisture-tracking products over most of the globe.

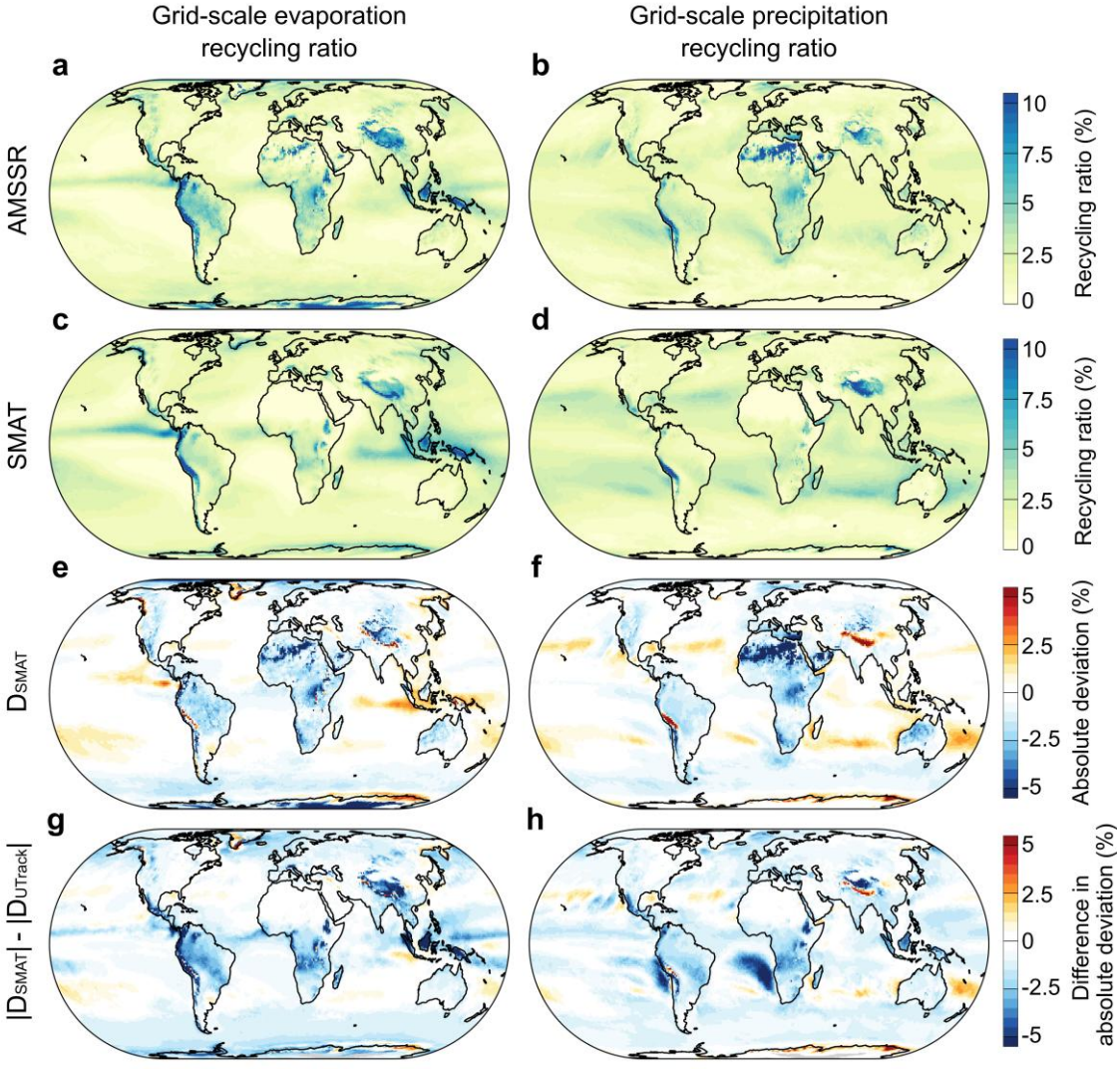


Figure 5. Evaluation of grid-scale moisture recycling ratios. (a, b) Evaporation recycling ratio (ERR) and precipitation recycling ratio (PRR) from the AMSSR reference dataset, respectively. (c, d) Same as (a, b), but for SMAT results. (e, f) Spatial distributions of the deviations between SMAT and AMSSR (D_{SMAT}) for ERR and PRR, respectively. (g, h) Differences between the absolute deviation of SMAT from AMSSR and the corresponding inter-model spread represented by UTrack ($|D_{\mathrm{SMAT}}|-|D_{\mathrm{UTrack}}|$) for ERR and PRR, respectively.

https://doi.org/10.5194/egusphere-2026-5716
Preprint. Discussion started: 11 November 2026
© Author(s) 2026. CC BY 4.0 License.

3.2 Basin-scale moisture recycling

In this section, we further examine the performance of SMAT in representing basin-scale moisture recycling ratios across the 26 largest river basins (Table 1). These basins cover major hydroclimatic regions worldwide, and their geographical locations are shown in Fig. A1. Accordingly, at the basin scale, the ERR and PRR are defined as follows:

$$\mathrm{ERR} = \frac{R_{\mathrm{local}\to\mathrm{basin}}}{E_{\mathrm{basin}}}, \mathrm{PRR} = \frac{R_{\mathrm{local}\to\mathrm{basin}}}{R_{\mathrm{basin}}}, \tag{18}$$

where $R_{\mathrm{local}\to\mathrm{basin}}$ denotes the amount of moisture originating from evaporation within the basin that is ultimately retained within the same basin, E_{basin} denotes the total evaporation from the basin, and R_{basin} denotes the total moisture retained within the basin from all source basins.

The results show that basin-scale moisture recycling varies substantially among the 26 major river basins (Table 1). High recycling ratios are generally found in large humid basins, including the Amazon, Congo, Ganges, and Yangtze, indicating strong recycling of locally evaporated moisture within these regions. By contrast, much lower recycling ratios occur in arid and semi-arid basins such as the Murray, Orange, and Tigris basins, where remotely transported atmospheric moisture plays a relatively larger role in the regional water budget. Across these basins, however, the level of agreement between SMAT and AMSSR is far from uniform. SMAT agrees particularly well with AMSSR in several northern high-latitude basins, including the Lena, Ob, Mackenzie, Amur, and Kolyma, as well as in monsoon-influenced basins such as the Yangtze and Niger, where its deviations are generally smaller than those of UTrack. Larger differences emerge in several humid basins with strong moisture recycling, notably the Amazon and Ganges, and in some arid basins, such as the Nile, Indus, and Chad. Taken together, these basin-to-basin differences yield an arithmetic mean absolute deviation from AMSSR across the 26 basins of 5.9% for ERR and 6.2% for PRR in SMAT, compared with 7.6% and 7.7%, respectively, in UTrack. Across the 26 basins, SMAT deviates less from the AMSSR than the UTrack does in 16 cases for both recycling metrics, further demonstrating its robust performance in representing basin-scale moisture recycling.

Table 1. Basin-scale evaluation of moisture recycling ratios across the 26 largest river basins.

River basin	Basin-scale evaporation recycling ratio (%)			Basin-scale precipitation recycling ratio (%)		
	AMSSR	SMAT	UTrack	AMSSR	SMAT	UTrack
Amazon	57.8	49.3	60.9	33.0	25.5	32.0
Congo	43.9	**34.9**	59.4	41.6	29.9	45.0
Mississippi	16.5	**20.4**	28.3	12.2	**15.9**	22.4
Nile	31.9	19.3	39.6	30.0	17.0	25.1
Paraná	28.6	23.6	32.2	25.4	18.5	24.9
Yenisej	26.9	19.8	32.6	13.6	**12.7**	25.8
Ob	16.2	**19.8**	25.8	10.4	**14.0**	22.2

https://doi.org/10.5194/egusphere-2026-5716
Preprint. Discussion started: 11 November 2026
© Author(s) 2026. CC BY 4.0 License.

Lena	27.3	**36.1**	38.3	13.9	**23.4**	31.7
Yangtze	26.5	**28.8**	38.2	16.6	**18.0**	25.9
Amur	16.8	**32.3**	36.1	12.4	**24.1**	31.1
Niger	13.5	**13.0**	21.4	12.0	**11.3**	16.6
Mackenzie	21.6	**17.8**	31.7	12.6	**18.5**	33.2
Ganges	39.7	48.3	36.9	16.9	25.2	17.3
Chad	13.8	9.0	18.1	14.8	8.7	18.0
Zambezi	24.2	**24.0**	25.8	19.6	**20.9**	21.5
Volga	11.5	18.5	17.4	7.5	**13.3**	15.8
Nelson	9.8	**14.5**	17.4	7.4	**12.9**	17.6
Murray	7.9	11.6	10.3	8.4	12.3	9.3
Lawrence	7.7	**15.9**	16.1	4.4	**10.7**	13.4
Orange	15.7	10.8	17.9	17.8	10.9	13.4
Tigris	4.2	**7.4**	9.8	3.9	**5.0**	5.2
Indus	31.8	25.2	33.1	21.9	31.4	25.3
Yukon	20.5	**17.8**	26.3	8.6	**17.4**	23.0
Danube	11.8	**19.9**	23.5	9.9	16.3	15.7
Huang	9.2	**15.0**	22.2	8.7	**17.8**	21.6
Kolyma	8.5	**12.2**	17.0	3.8	**8.4**	12.6
Mean absolute deviation		**5.9**	7.6		**6.2**	7.7

Bold values indicate that the deviations between SMAT and AMSSR are smaller than those between UTrack and AMSSR.

3.3 Continental-scale moisture recycling and source–sink relationships

Furthermore, we examine continental-scale moisture recycling ratios. Here, the continental-scale ERR is defined as the fraction of moisture evaporated from each land grid cell that is ultimately retained over global land, whereas the continental-scale PRR is defined as the fraction of moisture retained in each land grid cell that originates from evaporation over global land:

$$ERR = \frac{R_{i\to\mathrm{land}}}{E_i}, PRR = \frac{R_{\mathrm{land}\to i}}{R_i}, \quad (19)$$

where $R_{i\to\mathrm{land}}$ denotes the amount of moisture evaporated from grid cell i that is ultimately retained over global land, $R_{\mathrm{land}\to i}$ denotes the amount of moisture retained in grid cell i originating from evaporation over global land, E_i is the total evaporation from grid cell i, and R_i is the total moisture retained in grid cell i.

https://doi.org/10.5194/egusphere-2026-5716
Preprint. Discussion started: 11 November 2026
© Author(s) 2026. CC BY 4.0 License.

Extending the analysis from the basin scale to the global land surface reveals a clear contrast between the spatial organization of evaporation and precipitation recycling (Fig. 6a–d). Continental-scale ERR exhibits a broader and more spatially continuous distribution, with high values extending across Eurasia and the Amazon Basin, whereas PRR is more regionally concentrated, with pronounced values over eastern Eurasia and the Andes. SMAT reproduces this contrast well. The area-weighted mean of the grid-cell continental-scale ERR values over global land is 15.5% in SMAT and 16.2% in AMSSR, while the corresponding mean PRR values are 10.0% and 10.3%, respectively, further indicating close agreement in the overall magnitude of terrestrial moisture recycling. The differences between SMAT and AMSSR are mainly concentrated in several distinct regions rather than being widespread across the global land surface. For ERR, the most pronounced negative biases occur over northern China and the Mongolian Plateau, suggesting stronger moisture export from these regions in SMAT. For PRR, negative biases are primarily found over the Sahara–Arabian Peninsula and parts of the tropical monsoon regions, whereas both ERR and PRR tend to be overestimated across high-latitude Eurasia (Fig. 6e, f).

To further place SMAT deviations into context, we compared them with the corresponding deviations of UTrack relative to the AMSSR reference. SMAT yields area-weighted mean absolute grid-cell deviations of 3.21% for ERR and 4.16% for PRR, compared with 2.64% and 3.08%, respectively, for UTrack. The somewhat larger SMAT deviations are largely associated with pronounced regional biases over the Sahara, northern China, and the Mongolian Plateau. Outside these regions, the differences between SMAT and AMSSR are generally comparable in magnitude to those between UTrack and AMSSR. Taken together, the close agreement in the large-scale spatial patterns and area-weighted global land means indicates that SMAT provides a broadly consistent representation of terrestrial moisture recycling at the continental scale despite several regionally concentrated discrepancies (Fig. 6g, h).

https://doi.org/10.5194/egusphere-2026-5716
Preprint. Discussion started: 11 November 2026
© Author(s) 2026. CC BY 4.0 License.

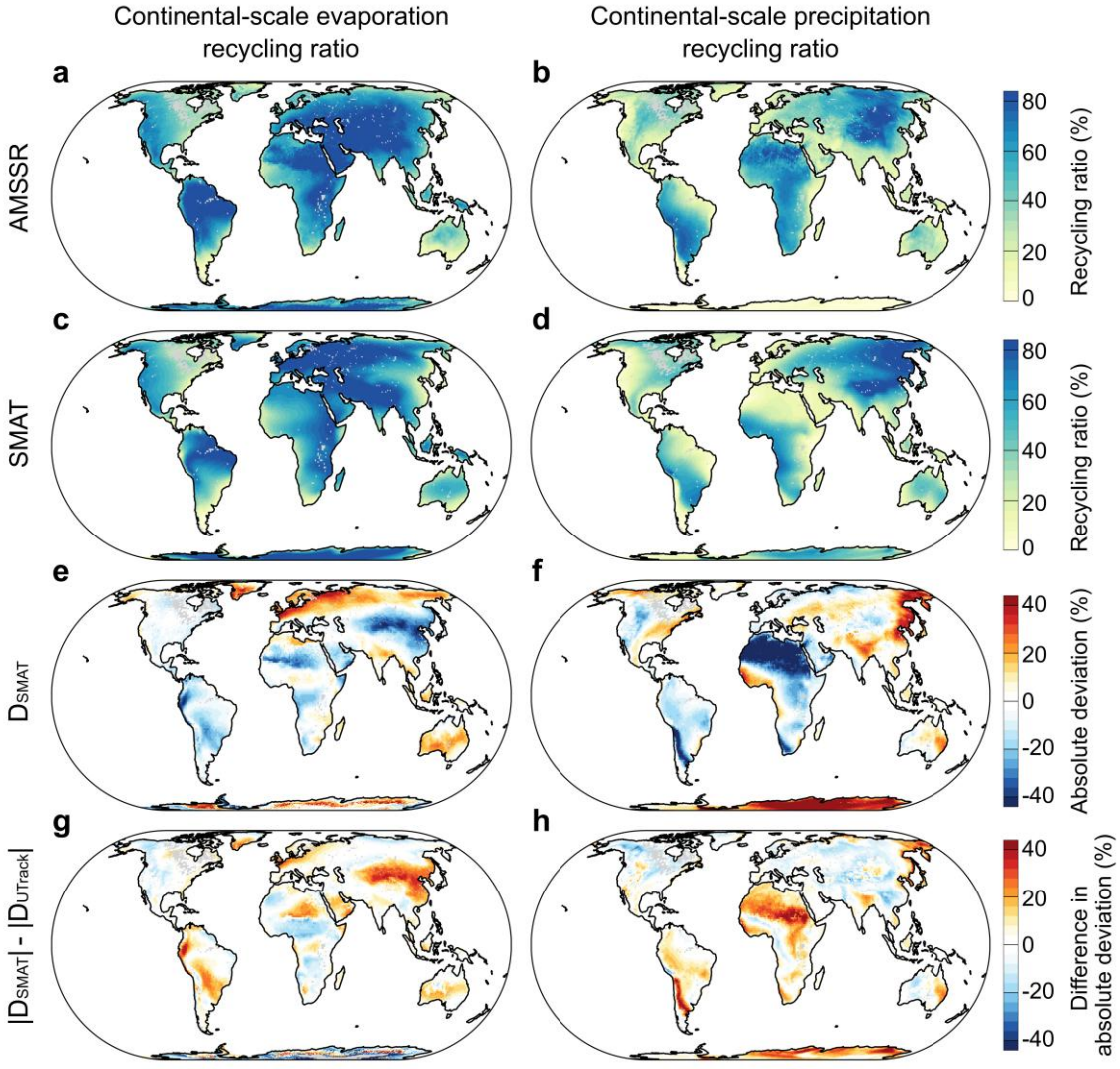


Figure 6. Evaluation of continental-scale moisture recycling ratios. (a, b) Continental-scale evaporation recycling ratio (ERR) and precipitation recycling ratio (PRR) from the AMSSR reference dataset, respectively. (c, d) Same as (a, b), but for SMAT. (e, f) Spatial distributions of the deviations between SMAT and AMSSR for ERR and PRR, respectively. (g, h) Differences between the absolute deviation of SMAT from AMSSR and the corresponding inter-model spread represented by UTrack ($|D_{SMAT}| - |D_{UTrack}|$) for the continental ERR and PRR, respectively.

We next examine global moisture source–sink relationships over land and ocean, considering both the origins of moisture received by land and ocean and the destinations of moisture evaporated from these domains (Fig. 7). From the sink perspective, we quantify the fractional contribution of each grid cell to the total moisture received by land or ocean ($\frac{R_{i\to land}}{R_{land}}$ and $\frac{R_{i\to ocean}}{R_{ocean}}$). From the source perspective, we quantify the fraction of total evaporation from land or ocean that is ultimately received by

https://doi.org/10.5194/egusphere-2026-5716
Preprint. Discussion started: 11 November 2026
© Author(s) 2026. CC BY 4.0 License.

each grid cell, expressed as $\frac{R_{\text{land}\to i}}{E_{\text{land}}}$ and $\frac{R_{\text{ocean}\to i}}{E_{\text{ocean}}}$, where R_{land} and R_{ocean} are the total moisture retained over land and ocean, respectively, and E_{land} and E_{ocean} are the corresponding total evaporation.

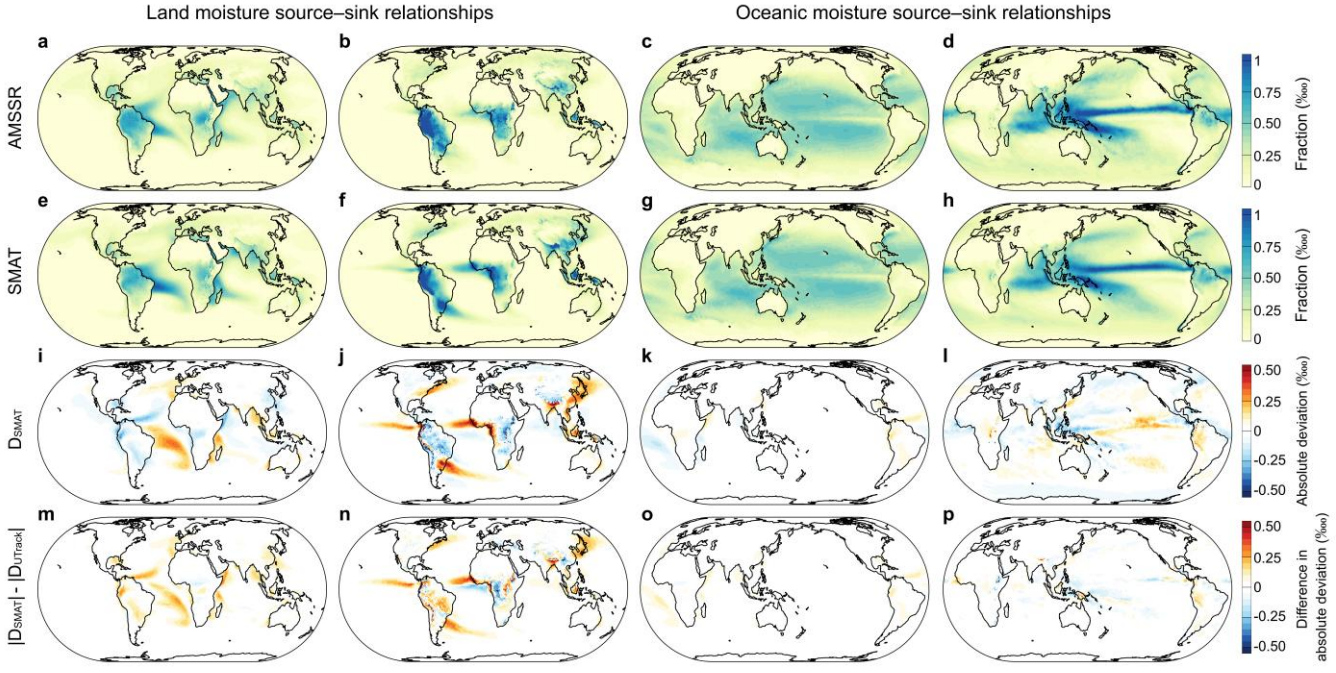


Figure 7. Evaluation of global land and oceanic moisture source–sink relationships. (a–d) Moisture sources (fractional contribution to moisture retained, first and third columns) and moisture sinks (fraction of evaporation ultimately retained, second and fourth columns) for the land (a, b) and ocean (c, d) in the AMSSR reference dataset. (e–h) Same as (a–d), but for SMAT. (i–l) Spatial deviations of SMAT from AMSSR (D_{SMAT}) for the moisture sources and sinks of the land (i, j) and ocean (k, l). (m–p) Differences between the absolute deviation of SMAT from AMSSR and the corresponding inter-model spread represented by UTrack ($| D_{SMAT} | - | D_{UTrack} |$) for the moisture sources and sinks of the land (m, n) and ocean (o, p).

As shown in Fig. 7, SMAT captures the large-scale organization of terrestrial moisture source–sink relationships represented by AMSSR. Terrestrial precipitation is sustained by two major moisture supply pathways: evapotranspiration from humid tropical land regions, particularly the Amazon and Congo basins, and moisture transported inland from the adjacent Atlantic and Indian Oceans by low-latitude trade winds and monsoonal circulations (Fig. 7a, e). Terrestrial evaporation, in turn, is partly recycled within these humid continental regions and partly exported toward the South Atlantic, South Indian Ocean, and equatorial Pacific (Fig. 7b, f). These dominant source and destination patterns are well reproduced by SMAT. The main discrepancies arise in the relative strength of individual transport pathways. Over the Amazon Basin, SMAT overestimates the contribution associated with the South Atlantic Convergence Zone while underestimating moisture transport linked to the northeasterly trade winds (Fig. 7i). A broader bias is evident in the fate of terrestrial evaporation, with SMAT tending to

https://doi.org/10.5194/egusphere-2026-5716
Preprint. Discussion started: 11 November 2026
© Author(s) 2026. CC BY 4.0 License.

underestimate local recycling over the Amazon and Congo basins while enhancing offshore moisture export and subsequent retention over the oceans (Fig. 7j). Nevertheless, these regional differences remain small in the global context, with mean absolute grid-cell deviations of 0.07 ‰ and 0.09 ‰ for the terrestrial moisture source and destination distributions, respectively, which are only slightly larger than the corresponding UTrack values of 0.04 ‰ and 0.06 ‰ (Fig. 7m, n).

Oceanic moisture transport shows an even closer agreement with the AMSSR. The dominant evaporation sources are concentrated within the subtropical high-pressure belts, particularly over the eastern Pacific, Atlantic, and South Indian Oceans (Fig. 7c, g), whereas the major destinations of oceanic evaporation form broad zonal bands along the Intertropical Convergence Zone and tropical warm-pool regions of the Atlantic, Indian, and western Pacific Oceans (Fig. 7d, h). SMAT reproduces this large-scale source–sink structure with substantially smaller deviations than those found over land. The remaining differences are mainly associated with the destinations of oceanic moisture, with an overestimation of retention over the central–eastern tropical Pacific and an underestimation over the Indian Ocean and western tropical Pacific (Fig. 7l). The mean absolute grid-cell deviations for the oceanic source and destination distributions are 0.02 ‰ and 0.05 ‰, respectively, compared with 0.01 ‰ and 0.05 ‰ for UTrack. These results indicate that SMAT reproduces the dominant oceanic moisture pathways at a level broadly consistent with the established UTrack product.

4 Seasonal cycle of moisture recycling

The preceding multi-scale evaluations demonstrate that SMAT successfully reproduces both the spatial characteristics of moisture recycling and the large-scale patterns of moisture source–sink relationships under climatological mean conditions. However, these evaluations do not assess the model's ability to reproduce temporal variability. To provide a comprehensive evaluation of SMAT, this section examines its ability to reproduce the seasonal cycle of moisture recycling at both the continental and basin scales. To minimize the influence of climatological mean biases on the evaluation of seasonal variability, the annual climatological mean is removed from each seasonal value:

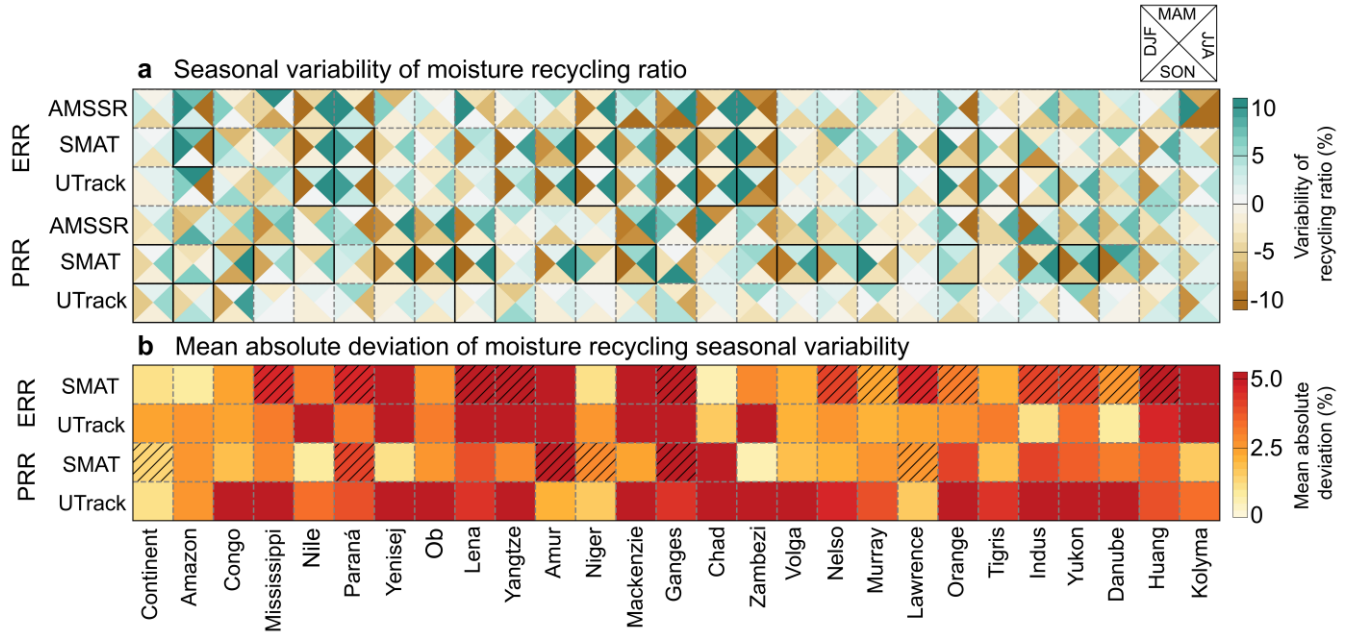
$$X'_{\text{season}} = X_{\text{season}} - \overline{X}\,, \tag{20}$$

where X_{season} is the climatological value for a given season, $\overline{X}$ is the corresponding annual climatological mean, and X'_{season} denotes the seasonal departure used in the subsequent evaluation. To further quantify the overall agreement of the seasonal variability with the AMSSR reference dataset, the mean absolute deviation of the seasonal variability (MADSV) is calculated as follows:

$$\text{MADSV} = \frac{1}{N}\sum_{s=1}^{N}\left|X_s'^{,\text{model}} - X_s'^{,\text{AMSSR}}\right|, \tag{21}$$

where $X_s'^{,\text{model}}$ and $X_s'^{,\text{AMSSR}}$ denote the seasonal variability metric for season s derived from the model (SMAT or UTrack) and AMSSR, respectively, and $N = 4$ is the number of climatological seasons. To additionally assess the consistency of the seasonal-cycle phase, a basin was considered consistent with AMSSR when the seasons corresponding to both the maximum and minimum seasonal anomalies were the same in the two datasets.

https://doi.org/10.5194/egusphere-2026-5716
Preprint. Discussion started: 11 November 2026
© Author(s) 2026. CC BY 4.0 License.



535 **Figure 8.** Seasonal variability in moisture recycling. (a) Seasonal anomalies of the evaporation recycling ratio (ERR) and precipitation recycling ratio (PRR) derived from the AMSSR benchmark dataset and simulated by SMAT and UTrack. The four triangles within each grid cell represent winter (DJF, left), spring (MAM, top), summer (JJA, right), and autumn (SON, bottom), as illustrated in the schematic at the upper right. Black solid outlines indicate river basins or land areas where the simulated seasonal cycle agrees with AMSSR in the timing of both the seasonal peak and trough. (b) Mean absolute deviation
540 of the simulated seasonal anomalies relative to AMSSR for SMAT and UTrack. Hatched cells indicate that the seasonal mean absolute deviation of SMAT exceeds that of UTrack (i.e., | SMAT − AMSSR |>| UTrack − AMSSR |). The results are shown for the global land average (leftmost column) and the 26 major river basins (remaining columns).

The results show that, at the continental scale, SMAT reproduces the major seasonal characteristics of both ERR and PRR
545 observed in the AMSSR benchmark dataset (Fig. 8a, first column). For ERR, both SMAT and AMSSR exhibit positive anomalies during JJA and negative anomalies during SON, reflecting enhanced land–atmosphere moisture recycling during the boreal warm season followed by a decline in autumn. In contrast, UTrack exhibits a slightly weaker positive anomaly during JJA and a longer-lasting negative phase. For PRR, both SMAT and UTrack reproduce the unimodal seasonal cycle in AMSSR, characterized by positive anomalies during JJA and negative anomalies during boreal winter. The comparison of the
550 mean absolute deviations relative to AMSSR (Fig. 8b) further supports these results. At the continental scale, the mean absolute deviation of the simulated seasonal ERR anomalies is 1.24% for SMAT, compared with 2.48% for UTrack. For PRR, the corresponding deviation is 1.38% for SMAT and 1.25% for UTrack, indicating that SMAT closely reproduces the seasonal evolution of continental moisture recycling, with deviations comparable to those represented by the existing inter-model spread.

https://doi.org/10.5194/egusphere-2026-5716
Preprint. Discussion started: 11 November 2026
© Author(s) 2026. CC BY 4.0 License.

At the basin scale, SMAT reproduces the seasonal variability in moisture recycling across the major river basins identified in the AMSSR benchmark dataset. For ERR, the strongest seasonal variability is found primarily in the Ganges, Indus, Yangtze, Huang He, Niger, and Paraná basins, where SMAT successfully reproduces both the sign and relative magnitude of the seasonal anomalies. SMAT reproduces the timing of both the seasonal peak and trough in AMSSR in 8 of the 26 basins, comparable to the 9 basins reproduced by UTrack. Compared with UTrack, the absolute deviation of SMAT relative to AMSSR exceeds the corresponding UTrack–AMSSR deviation in 13 of the 26 basins. For PRR, SMAT reproduces the seasonal variability across most major river basins, maintaining close agreement with AMSSR in both the magnitude and spatial distribution of seasonal anomalies. Notably, SMAT reproduces the timing of the seasonal peak and trough in AMSSR in 13 basins, substantially more than UTrack, which reproduces them in only 2 basins. Only 5 of the 26 basins exhibit larger SMAT–AMSSR deviations than the corresponding UTrack–AMSSR deviations, indicating that the simulation errors of SMAT generally remain within the range of inter-model differences among existing atmospheric moisture-tracking approaches. Overall, these results demonstrate that SMAT provides a robust representation of seasonal moisture recycling across multiple spatial scales, with performance broadly comparable to that of UTrack.

5 Summary and discussion

In this study, we develop the sparse matrix-based atmospheric moisture tracking (SMAT) model, which reformulates atmospheric moisture transport into a sparse linear system based on local moisture partitioning and a global transport network. This formulation avoids explicit Lagrangian trajectory integration while enabling efficient diagnosis of climatological moisture source–sink relationships. Compared with conventional moisture-tracking approaches, which typically require weeks to months or even longer for long-term simulations, SMAT substantially reduces the computational cost, shortening the computation time to only a few hours or even minutes. This substantial increase in computational efficiency makes SMAT a practical tool for investigating moisture recycling, land–atmosphere interactions, and hydrological teleconnections, particularly in large-ensemble climate simulations and future climate change assessments.

Multi-scale evaluation against the AMSSR benchmark dataset, complemented by inter-model comparison with the UTrack model, demonstrates that SMAT closely reproduces evaporation and precipitation recycling ratios from the grid to the basin and continental scales. At the grid scale, SMAT successfully identifies strong moisture recycling centres over tropical rainforest regions such as the Amazon and Congo basins, as well as orography-driven local feedbacks around the Andes and the Tibetan Plateau, in agreement with the findings of previous studies (van der Ent et al., 2010; Tuinenburg et al., 2020; Theeuwen et al., 2023). At the basin and continental scales, the model clearly captures water-cycle characteristics and key moisture transport pathways across major river systems, while reproducing large-scale inland moisture recycling patterns and the global land–ocean source–sink structure, which is consistent with the established hydroclimatic understanding (Goessling

https://doi.org/10.5194/egusphere-2026-5716
Preprint. Discussion started: 11 November 2026
© Author(s) 2026. CC BY 4.0 License.

and Reick, 2013; Link et al., 2020; Tuinenburg et al., 2020). At the temporal scale, SMAT accurately reproduces the seasonal variability in moisture recycling across both continental and basin scales. At the continental scale, it captures the characteristic seasonal evolution of both evaporation and precipitation recycling, reproducing the positive summer anomalies and autumn decline in evaporation recycling together with the unimodal seasonal cycle of precipitation recycling, which is consistent with previous work (Tuinenburg et al., 2020). The model also successfully reproduces the strongest seasonal variability over major monsoon-influenced river basins, suggesting that SMAT generally performs within the range of inter-model differences represented by UTrack.

Despite its good agreement in reproducing large-scale climatological moisture source–sink relationships, SMAT relies on several simplifying assumptions to improve computational efficiency, which inevitably introduce uncertainties and constrain its applicable timescales. First, SMAT assumes that atmospheric moisture is vertically well mixed within each grid cell, simplifying three-dimensional moisture transport into a two-dimensional transfer process based on vertically integrated transport fields. In reality, moisture and horizontal winds can exhibit substantial vertical heterogeneity, particularly under strong vertical wind shear, potentially smoothing or shifting actual transport pathways and introducing uncertainties in local and regional moisture source–sink estimates (Goessling and Reick, 2013; van der Ent et al., 2013; Keys et al., 2014; Dominguez et al., 2016; Dominguez et al., 2020). Furthermore, the transport network of SMAT is constructed from long-term mean atmospheric circulation, which captures persistent transport patterns but filters the transient variability associated with weather systems and circulation anomalies. Consequently, its capability to resolve short-term moisture transport adjustments and extreme transport events at sub-seasonal to seasonal timescales is limited. These uncertainties decrease with increasing analysis periods, as longer-term averaging enhances the representation of persistent moisture transport characteristics and suppresses the influence of high-frequency variability (Seager et al., 2010; Liu et al., 2021). Therefore, in practice, we recommend that SMAT be applied over multi-year periods, particularly for interannual and longer-term analyses, where diagnosed source–sink relationships primarily reflect statistically persistent climatological signals rather than transient meteorological variability.

https://doi.org/10.5194/egusphere-2026-5716
Preprint. Discussion started: 11 November 2026
© Author(s) 2026. CC BY 4.0 License.

Appendix A: Geographic distribution of the 26 major river basins

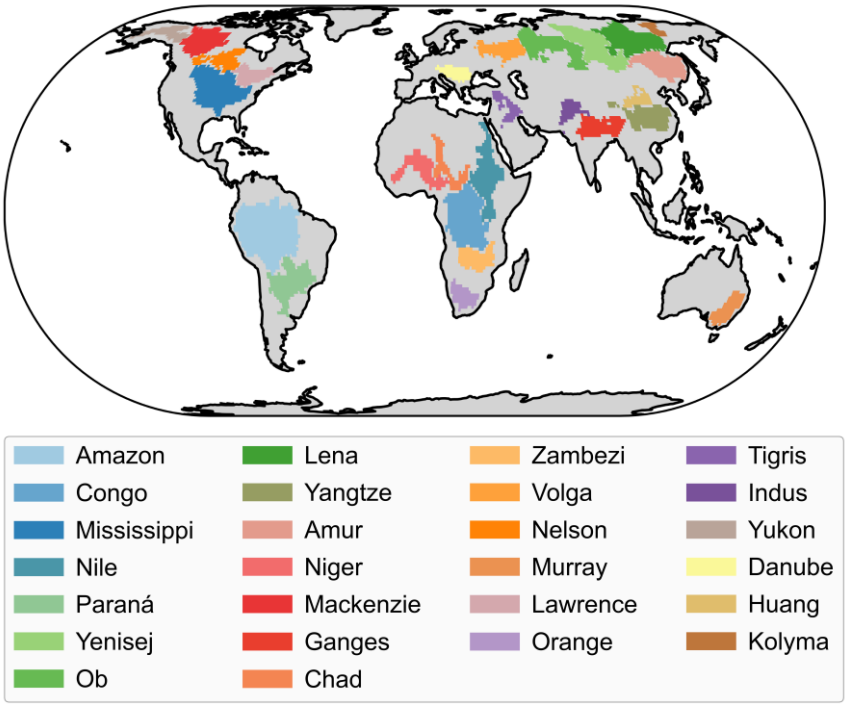


Figure A1. Geographic distribution of the 26 major river basins analysed in this study. Different colours denote individual river basins, and the corresponding basin names are provided in the legend.

Appendix B: Characteristics of local moisture partitioning in SMAT

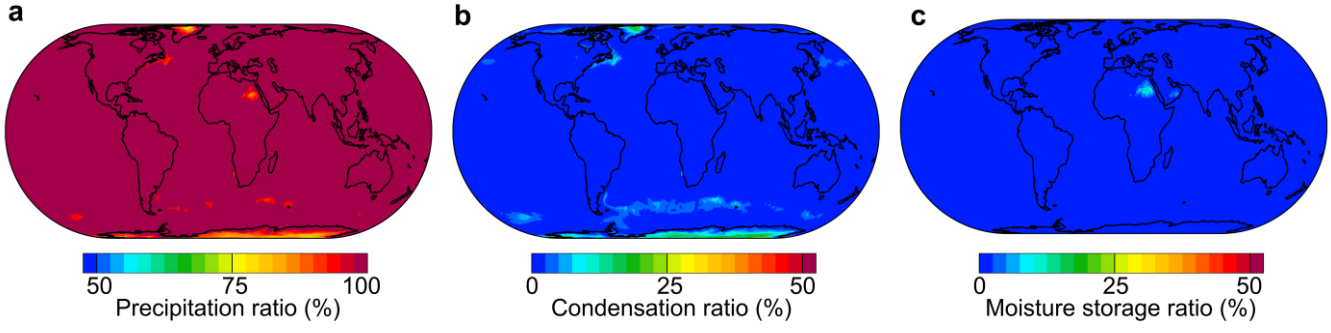
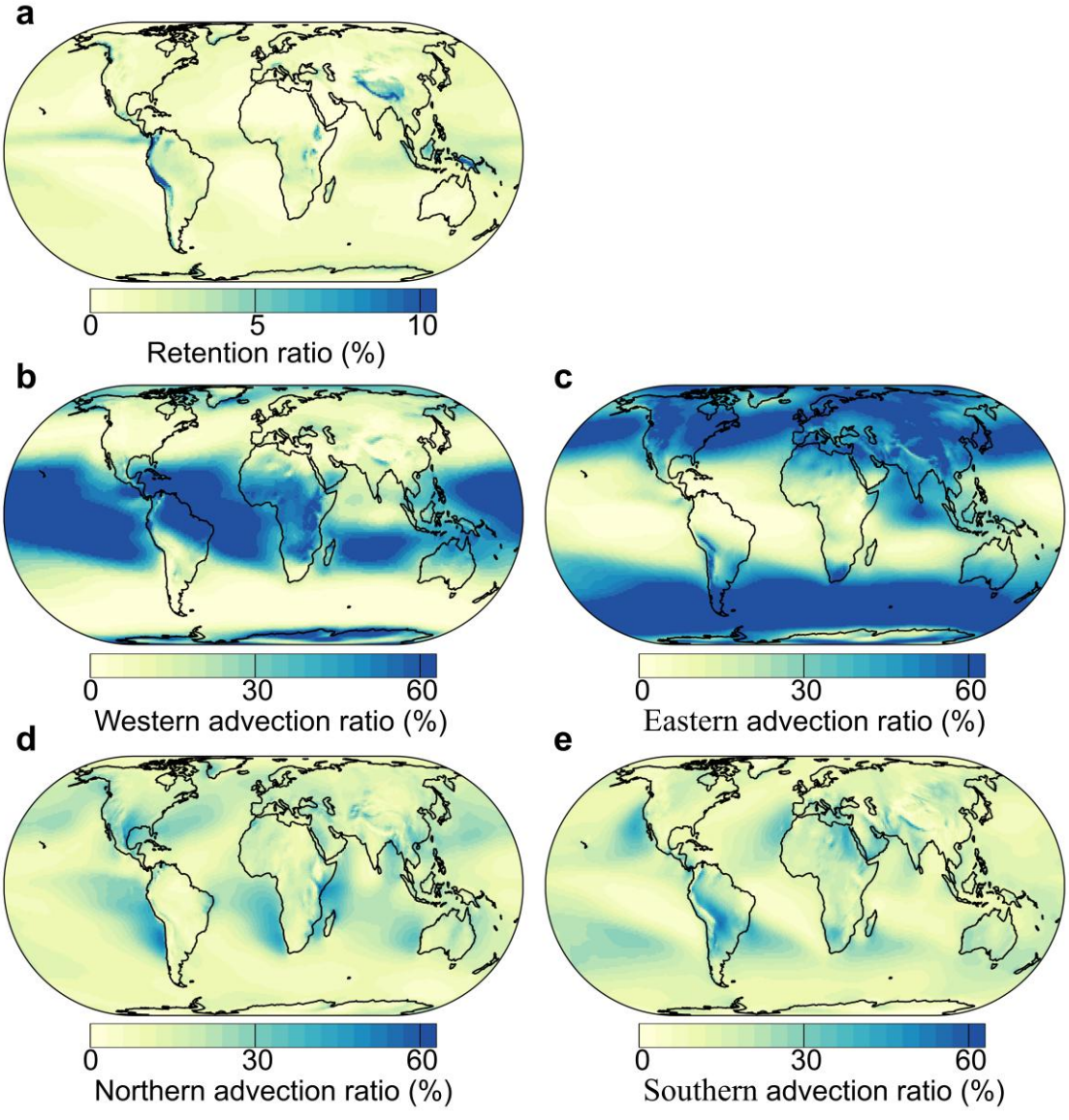


Figure B1. Fractional contributions of local moisture sink processes to the total retention probability. Spatial distributions of the proportion of the retention probability driven by (a) precipitation, (b) condensation, and (c) changes in atmospheric moisture storage.

https://doi.org/10.5194/egusphere-2026-5716
Preprint. Discussion started: 11 November 2026
© Author(s) 2026. CC BY 4.0 License.



620

Figure B2. Spatial distributions of local moisture partitioning probabilities. (a) Internal retention probability. (b–e) Directional export probabilities to the northern, southern, western, and eastern neighbouring grid cells, respectively. These probabilities satisfy the local mass balance constraint.

https://doi.org/10.5194/egusphere-2026-5716
Preprint. Discussion started: 11 November 2026
© Author(s) 2026. CC BY 4.0 License.

Appendix C: Spatial Patterns of UTrack Moisture Recycling

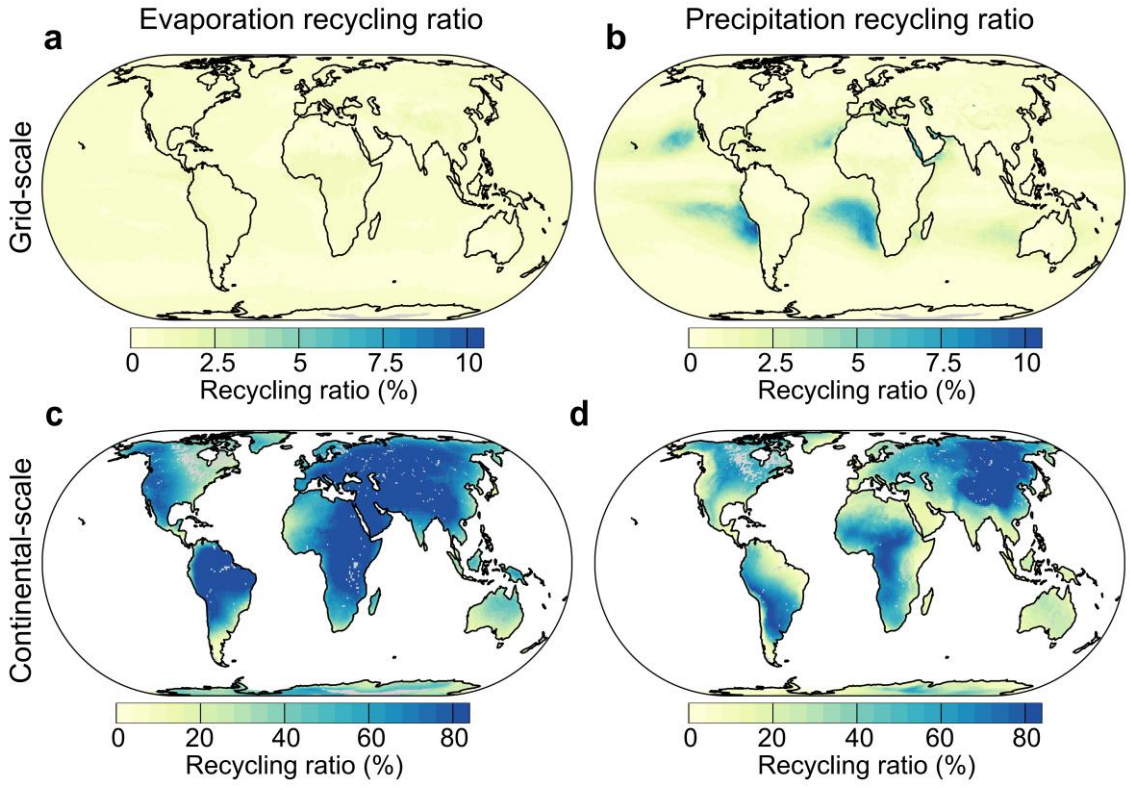


Figure C1. Climatological evaporation and precipitation recycling ratios derived from the UTrack dataset. (a, b) Grid-cell evaporation and precipitation recycling ratios. (c, d) Continental evaporation and precipitation recycling ratios. All fields represent the 2008–2017 climatology.

https://doi.org/10.5194/egusphere-2026-5716
Preprint. Discussion started: 11 November 2026
© Author(s) 2026. CC BY 4.0 License.

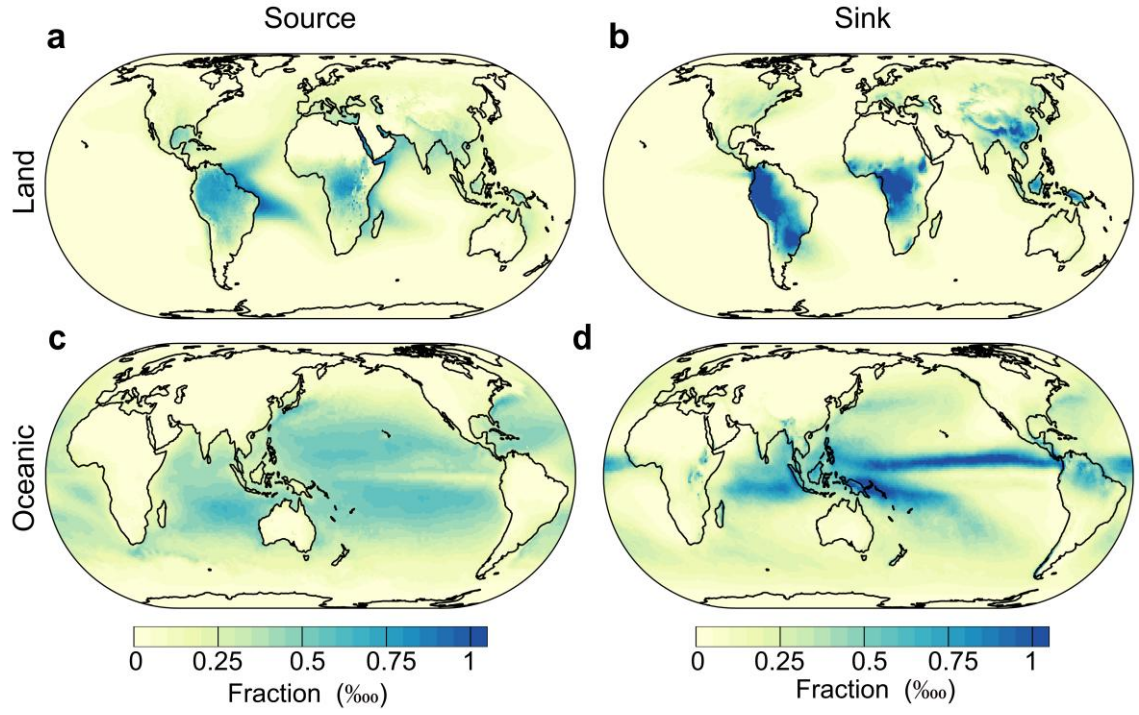


Figure C2. Climatological atmospheric moisture source–sink relationships derived from the UTrack dataset. (a, b) Moisture sources (fractional contribution to moisture retained) and moisture sinks (fraction of evaporation ultimately retained) for land. (c, d) Same as (a, b), but for ocean. All fields represent the 2008–2017 climatology.

Code and data availability

The datasets generated and processed in this study, together with the scripts used to reproduce the analyses and figures presented in this paper, are available at https://doi.org/10.5281/zenodo.22810352 (Shan, 2026b). The source code of the SMAT model is openly available at https://gitee.com/Smat-Main/smat/, which provides access to the latest development version and supports issue reporting and feature requests. The exact version of the SMAT model used in this study is archived on Zenodo at https://doi.org/10.5281/zenodo.22844093 (Shan, 2026a). The AMSSR dataset used as the benchmark dataset and the UTrack dataset used for comparison are publicly available from their respective data repositories at https://doi.org/10.11888/Atmos.tpdc.300478 and https://doi.pangaea.de/10.1594/PANGAEA.912710, respectively. ERA5 reanalysis data used to provide the atmospheric and surface variables required to drive the SMAT model were obtained from the Copernicus Climate Change Service (C3S) Climate Data Store at https://cds.climate.copernicus.eu/datasets/.

https://doi.org/10.5194/egusphere-2026-5716
Preprint. Discussion started: 11 November 2026
© Author(s) 2026. CC BY 4.0 License.

Author contributions

Conceptualization, Y.S., D.Q. and J.G.; methodology, Y.S.; software, Y.S.; validation, Y.S.; formal analysis, Y.S.; investigation, Y.S. and P.Q.; data curation, Y.S.; writing—original draft preparation, Y.S.; writing—review and editing, Y.S., J.G., K.Y., J.W., P.Q., D.Q., and F.L.; visualization, Y.S.; supervision, J.G.; project administration, J.G.; funding acquisition, J.G.; all authors have read and agreed to the published version of the manuscript.

Competing interests

The authors declare no conflicts of interest.

Acknowledgements

We sincerely thank Dr. Yu Liu and Dr. Yuanyuan Song for their valuable discussions and constructive suggestions throughout the development of this work. Their comments and insights were helpful in refining the methodological framework, interpreting the results, and improving the clarity and presentation of the manuscript. We are grateful for their time and thoughtful feedback during the course of this study.

Financial support

Jun Ge was supported by the Fundamental and Interdisciplinary Disciplines Breakthrough Plan of the Ministry of Education of China (grant no. JYB2025XDXM907) and the Natural Science Foundation of Jiangsu Province (grant no. BK20240170). Dongdong Qiu was supported by the National Natural Science Foundation of China (grant no. 425B2034).

References

Cui, J., Lian, X., Huntingford, C., Gimeno, L., Wang, T., Ding, J., He, M., Xu, H., Chen, A., Gentine, P., and Piao, S.: Global water availability boosted by vegetation-driven changes in atmospheric moisture transport, Nature Geoscience, 15, 982–988, https://doi.org/10.1038/s41561-022-01061-7, 2022.

Dirmeyer, P. A. and Brubaker, K. L.: Contrasting evaporative moisture sources during the drought of 1988 and the flood of 1993, Journal of Geophysical Research: Atmospheres, 104, 19383–19397, https://doi.org/10.1029/1999jd900222, 1999.

Dominguez, F., Kumar, P., Liang, X.-Z., and Ting, M.: Impact of Atmospheric Moisture Storage on Precipitation Recycling, Journal of Climate, 19, 1513–1530, https://doi.org/10.1175/jcli3691.1, 2006.

https://doi.org/10.5194/egusphere-2026-5716
Preprint. Discussion started: 11 November 2026
© Author(s) 2026. CC BY 4.0 License.

Dominguez, F., Miguez-Macho, G., and Hu, H.: WRF with Water Vapor Tracers: A Study of Moisture Sources for the North American Monsoon, Journal of Hydrometeorology, 17, 1915–1927, https://doi.org/10.1175/jhm-d-15-0221.1, 2016.

Dominguez, F., Hu, H., and Martinez, J. A.: Two-Layer Dynamic Recycling Model (2L-DRM): Learning from Moisture Tracking Models of Different Complexity, Journal of Hydrometeorology, 21, 3–16, https://doi.org/10.1175/jhm-d-19-0101.1, 2020.

Dominguez, F., Eiras-Barca, J., Yang, Z., Bock, D., Nieto, R., and Gimeno, L.: Amazonian Moisture Recycling Revisited Using WRF With Water Vapor Tracers, Journal of Geophysical Research: Atmospheres, 127, e2021JD035259, https://doi.org/10.1029/2021jd035259, 2022.

Findell, K. L., Keys, P. W., van der Ent, R. J., Lintner, B. R., Berg, A., and Krasting, J. P.: Rising Temperatures Increase Importance of Oceanic Evaporation as a Source for Continental Precipitation, Journal of Climate, 32, 7713–7726, https://doi.org/10.1175/jcli-d-19-0145.1, 2019.

Gimeno, L., Stohl, A., Trigo, R. M., Dominguez, F., Yoshimura, K., Yu, L., Drumond, A., Durán-Quesada, A. M., and Nieto, R.: Oceanic and terrestrial sources of continental precipitation, Reviews of Geophysics, 50, RG4001, https://doi.org/10.1029/2012rg000389, 2012.

Gimeno, L., Nieto, R., and Sorí, R.: The growing importance of oceanic moisture sources for continental precipitation, npj Climate and Atmospheric Science, 3, 27, https://doi.org/10.1038/s41612-020-00133-y, 2020.

Goessling, H. F. and Reick, C. H.: On the "well-mixed" assumption and numerical 2-D tracing of atmospheric moisture, Atmospheric Chemistry and Physics, 13, 5567–5585, https://doi.org/10.5194/acp-13-5567-2013, 2013.

Insua-Costa, D. and Miguez-Macho, G.: A new moisture tagging capability in the Weather Research and Forecasting model: formulation, validation and application to the 2014 Great Lake-effect snowstorm, Earth System Dynamics, 9, 167–185, https://doi.org/10.5194/esd-9-167-2018, 2018.

Insua-Costa, D., Miguez-Macho, G., and Llasat, M. C.: Local and remote moisture sources for extreme precipitation: a study of the two catastrophic 1982 western Mediterranean episodes, Hydrology and Earth System Sciences, 23, 3885–3900, https://doi.org/10.5194/hess-23-3885-2019, 2019.

https://doi.org/10.5194/egusphere-2026-5716
Preprint. Discussion started: 11 November 2026
© Author(s) 2026. CC BY 4.0 License.

Kalverla, P., Benedict, I., Weijenborg, C., and van der Ent, R. J.: Atmospheric moisture tracking with WAM2layers v3, Geoscientific Model Development, 18, 4335–4352, https://doi.org/10.5194/gmd-18-4335-2025, 2025.

Keys, P. W., van der Ent, R. J., Gordon, L. J., Hoff, H., Nikoli, R., and Savenije, H. H. G.: Analyzing precipitationsheds to understand the vulnerability of rainfall dependent regions, Biogeosciences, 9, 733–746, https://doi.org/10.5194/bg-9-733-2012, 2012.

Keys, P. W., Barnes, E. A., van der Ent, R. J., and Gordon, L. J.: Variability of moisture recycling using a precipitationshed framework, Hydrology and Earth System Sciences, 18, 3937–3950, https://doi.org/10.5194/hess-18-3937-2014, 2014.

Li, Y., Wang, C., Tang, Q., Yao, S., Sun, B., Peng, H., and Xiao, S.: Unraveling the discrepancies between Eulerian and Lagrangian moisture tracking models in monsoon- and westerly-dominated basins of the Tibetan Plateau, Atmospheric Chemistry and Physics, 24, 10741–10758, https://doi.org/10.5194/acp-24-10741-2024, 2024.

Link, A., van der Ent, R., Berger, M., Eisner, S., and Finkbeiner, M.: The fate of land evaporation – a global dataset, Earth System Science Data, 12, 1897–1912, https://doi.org/10.5194/essd-12-1897-2020, 2020.

Liu, Q., Li, T., and Zhou, W.: Impacts of Multi-Timescale Circulations on Meridional Moisture Transport, Journal of Climate, 34, 8065–8085, https://doi.org/10.1175/jcli-d-20-0126.1, 2021.

Liu, Y., Ge, J., Guo, W., Cao, Y., Chen, C., Luo, X., Yang, L., and Wang, S.: Revisiting Biophysical Impacts of Greening on Precipitation Over the Loess Plateau of China Using WRF With Water Vapor Tracers, Geophysical Research Letters, 50, e2023GL102809, https://doi.org/10.1029/2023gl102809, 2023.

Liu, Y., Spracklen, D. V., Parker, D. J., Holden, J., Ge, J., and Guo, W.: Recent Forest Loss in the Brazilian Amazon Causes Substantial Reductions in Dry Season Precipitation, AGU Advances, 6, e2025AV001670, https://doi.org/10.1029/2025av001670, 2025.

Lovejoy, T. E. and Nobre, C.: Amazon Tipping Point, Science Advances, 4, eaat2340, https://doi.org/10.1126/sciadv.aat2340, 2018.

Makarieva, A. M. and Gorshkov, V. G.: Biotic pump of atmospheric moisture as driver of the hydrological cycle on land, Hydrology and Earth System Sciences, 11, 1013–1033, https://doi.org/10.5194/hess-11-1013-2007, 2007.

https://doi.org/10.5194/egusphere-2026-5716
Preprint. Discussion started: 11 November 2026
© Author(s) 2026. CC BY 4.0 License.

Meier, R., Schwaab, J., Seneviratne, S. I., Sprenger, M., Lewis, E., and Davin, E. L.: Empirical estimate of forestation-induced precipitation changes in Europe, Nature Geoscience, 14, 473–478, https://doi.org/10.1038/s41561-021-00773-6, 2021.

Miguez-Macho, G., Rios-Entenza, A., and Dominguez, F.: The impact of soil moisture and evapotranspiration fluxes on the spring water cycle in the Iberian Peninsula: a study with moisture tracers in WRF, AGU Fall Meeting Abstracts, H12B-05, 2013.

Nusbaumer, J., Wong, T. E., Bardeen, C., and Noone, D.: Evaluating hydrological processes in the Community Atmosphere Model Version 5 (CAM5) using stable isotope ratios of water, Journal of Advances in Modeling Earth Systems, 9, 949–977, https://doi.org/10.1002/2016ms000839, 2017.

Pan, C., Zhu, B., Gao, J., and Kang, H.: Source apportionment of atmospheric water over East Asia – a source tracer study in CAM5.1, Geoscientific Model Development, 10, 673–688, https://doi.org/10.5194/gmd-10-673-2017, 2017.

Pranindita, A., Wang-Erlandsson, L., Fetzer, I., and Teuling, A. J.: Moisture recycling and the potential role of forests as moisture source during European heatwaves, Climate Dynamics, 58, 609–624, https://doi.org/10.1007/s00382-021-05921-7, 2022.

Qian, P., Zhu, B., Zhu, T., Fang, C., Lu, C., Chen, H., and Liao, H.: Terrestrial moisture sources dominate summer precipitation fluctuations in Northwest China, Environmental Research Letters, 19, 124052, https://doi.org/10.1088/1748-9326/ad8b5e, 2024.

Rockström, J., Mazzucato, M., Andersen, L. S., Fahrländer, S. F., and Gerten, D.: Why we need a new economics of water as a common good, Nature, 615, 794–797, https://doi.org/10.1038/d41586-023-00800-z, 2023.

Seager, R., Naik, N., and Vecchi, G. A.: Thermodynamic and Dynamic Mechanisms for Large-Scale Changes in the Hydrological Cycle in Response to Global Warming, Journal of Climate, 23, 4651–4668, https://doi.org/10.1175/2010jcli3655.1, 2010.

Shan, Y.: Source Code of the Sparse Matrix-based Atmospheric Moisture Tracking (SMAT) Model, Zenodo, https://doi.org/10.5281/zenodo.22844093, 2026a.

Shan, Y.: Code and data for “An efficient model for diagnosing global climatological moisture source–sink relationships”, Zenodo, https://doi.org/10.5281/zenodo.22810352, 2026b.

https://doi.org/10.5194/egusphere-2026-5716
Preprint. Discussion started: 11 November 2026
© Author(s) 2026. CC BY 4.0 License.

Silvério, D. V., Brando, P. M., Macedo, M. N., Beck, P. S. A., Bustamante, M., and Coe, M. T.: Agricultural expansion dominates climate changes in southeastern Amazonia: the overlooked non-GHG forcing, Environmental Research Letters, 10, 104015, https://doi.org/10.1088/1748-9326/10/10/104015, 2015.

Sodemann, H., Schwierz, C., and Wernli, H.: Interannual variability of Greenland winter precipitation sources: Lagrangian moisture diagnostic and North Atlantic Oscillation influence, Journal of Geophysical Research: Atmospheres, 113, D03104, https://doi.org/10.1029/2007jd008503, 2008.

Song, Y., Wei, J., Cheng, H., and Zan, B.: Irrigation in the North China plain regulates the diurnal cycle of precipitation and regional water cycle, Climate Dynamics, 62, 6329–6346, https://doi.org/10.1007/s00382-024-07208-z, 2024.

Staal, A., Fetzer, I., Wang-Erlandsson, L., Bosmans, J. H. C., Dekker, S. C., van Nes, E. H., Rockström, J., and Tuinenburg, O. A.: Hysteresis of tropical forests in the 21st century, Nature Communications, 11, 4978, https://doi.org/10.1038/s41467-020-18728-7, 2020a.

Staal, A., Flores, B. M., Aguiar, A. P. D., Bosmans, J. H. C., Fetzer, I., and Tuinenburg, O. A.: Feedback between drought and deforestation in the Amazon, Environmental Research Letters, 15, 044024, https://doi.org/10.1088/1748-9326/ab738e, 2020b.

Stohl, A. and James, P.: A Lagrangian Analysis of the Atmospheric Branch of the Global Water Cycle. Part I: Method Description, Validation, and Demonstration for the August 2002 Flooding in Central Europe, Journal of Hydrometeorology, 5, 656–678, https://doi.org/10.1175/1525-7541(2004)005<0656:alaota>2.0.co;2, 2004.

Theeuwen, J. J. E., Staal, A., Tuinenburg, O. A., Hamelers, B. V. M., and Dekker, S. C.: Local moisture recycling across the globe, Hydrology and Earth System Sciences, 27, 1457–1476, https://doi.org/10.5194/hess-27-1457-2023, 2023.

Tuinenburg, O. A. and Staal, A.: Tracking the global flows of atmospheric moisture and associated uncertainties, Hydrology and Earth System Sciences, 24, 2419–2435, https://doi.org/10.5194/hess-24-2419-2020, 2020.

Tuinenburg, O. A., Theeuwen, J. J. E., and Staal, A.: High-resolution global atmospheric moisture connections from evaporation to precipitation, Earth System Science Data, 12, 3177–3188, https://doi.org/10.5194/essd-12-3177-2020, 2020.

van der Ent, R. J. and Savenije, H. H. G.: Oceanic sources of continental precipitation and the correlation with sea surface temperature, Water Resources Research, 49, 3993–4004, https://doi.org/10.1002/wrcr.20296, 2013.

https://doi.org/10.5194/egusphere-2026-5716
Preprint. Discussion started: 11 November 2026
© Author(s) 2026. CC BY 4.0 License.

van der Ent, R. J., Savenije, H. H. G., Schaefli, B., and Steele-Dunne, S. C.: Origin and fate of atmospheric moisture over continents, Water Resources Research, 46, W09525, https://doi.org/10.1029/2010wr009127, 2010.

van der Ent, R. J., Tuinenburg, O. A., Knoche, H.-R., Kunstmann, H., and Savenije, H. H. G.: Should we use a simple or complex model for moisture recycling and atmospheric moisture tracking?, Hydrology and Earth System Sciences, 17, 4869–4884, https://doi.org/10.5194/hess-17-4869-2013, 2013.

Vázquez, M., Alvarez-Socorro, G., Fernández-Alvarez, J. C., Nieto, R., and Gimeno, L.: Global FLEXPART-ERA5 simulations using 30 million atmospheric parcels since 1980, Zenodo, https://doi.org/10.5281/zenodo.12204016, 2024.

Wang-Erlandsson, L., Fetzer, I., Keys, P. W., van der Ent, R. J., Savenije, H. H. G., and Gordon, L. J.: Remote land use impacts on river flows through atmospheric teleconnections, Hydrology and Earth System Sciences, 22, 4311–4328, https://doi.org/10.5194/hess-22-4311-2018, 2018.

Wang, J., Feng, J., and Yan, Z.: Impact of Extensive Urbanization on Summertime Rainfall in the Beijing Region and the Role of Local Precipitation Recycling, Journal of Geophysical Research: Atmospheres, 123, 3323–3340, https://doi.org/10.1002/2017jd027725, 2018.

Wang, S., Ge, J., Cao, Y., Liu, Y., Luo, X., Yang, L., Xiao, S., Miao, X., and Guo, W.: Divergent Hydrological Effects of Revegetation over the Chinese Loess Plateau Driven by East Asian Summer Monsoon Variability, Journal of Climate, 38, 5349–5369, https://doi.org/10.1175/jcli-d-24-0600.1, 2025.

Wei, J. and Dirmeyer, P. A.: Sensitivity of land precipitation to surface evapotranspiration: a nonlocal perspective based on water vapor transport, Geophysical Research Letters, 46, 12588–12597, https://doi.org/10.1029/2019gl085613, 2019.

Xie, D., Zhang, Y., Zhang, M., Tian, Y., Cao, Y., Mei, Y., Liu, S., and Zhong, D.: Hydrological impacts of vegetation cover change in China through terrestrial moisture recycling, Science of The Total Environment, 915, 170015, https://doi.org/10.1016/j.scitotenv.2024.170015, 2024.

Zan, B., Ge, J., Mu, M., Sun, Q., Luo, X., and Wei, J.: Spatiotemporal inequality in land water availability amplified by global tree restoration, Nature Water, 2, 863–874, https://doi.org/10.1038/s44221-024-00296-5, 2024.

https://doi.org/10.5194/egusphere-2026-5716
Preprint. Discussion started: 11 November 2026
© Author(s) 2026. CC BY 4.0 License.



Zemp, D. C., Schleussner, C.-F., Barbosa, H. M. J., Hirota, M., Montade, V., Sampaio, G., Staal, A., Wang-Erlandsson, L., and Rammig, A.: Self-amplified Amazon forest loss due to vegetation-atmosphere feedbacks, Nature Communications, 8, 14681, https://doi.org/10.1038/ncomms14681, 2017.

Zhang, Y., Zhong, D., Cai, R., Zhang, M., Tian, Y., Xie, D., Cao, Y., and Mei, Y.: A multi-model based dataset of global atmospheric moisture source-sink relationships and atmospheric basins, Scientific Data, 12, 1842, https://doi.org/10.1038/s41597-025-06123-0, 2025.